Available online at www.sciencedirect.com
SCIENCE DIRECT®
ELSEVIER
International Journal of Solids and Structures 42 (2005) 3918–3952
INTERNATIONAL JOURNAL OF SOLIDS and STRUCTURES
www.elsevier.com/locate/ijsolstr

Irreversible thermodynamics of triple junctions during the intergranular void motion under the electromigration forces

Tarik Omer Ogurtani *, Ersin Emre Oren

Department of Metallurgical and Materials Engineering, Middle East Technical University, 06531 Ankara, Turkey

Received 18 November 2003; received in revised form 17 November 2004
Available online 5 January 2005

Abstract

A rigorous reformulation of internal entropy production and the rate of entropy flow is developed for multi-component systems consisting of heterophases, interfaces and/or surfaces. The result is a well-posed moving boundary value problem describing the dynamics of curved interfaces and surfaces associated with voids and/or cracks that are intersected by grain boundaries. Extensive computer simulations are performed for void configuration evolution during intergranular motion. In particular we simulate evolution resulting from the action of capillary and electromigration forces in thin film metallic interconnects having a "bamboo" structure, characterized by grain boundaries aligned perpendicular to the free surface of the metallic film interconnects. Analysis of experimental data utilizing previously derived mean time to failure formulas gives consistent values for interface diffusion coefficients and enthalpies of voids. $3.0 \times 10^{-6}\exp(-0.62\ \mathrm{eV}/kT)\ \mathrm{m}^2\ \mathrm{s}^{-1}$ is the value obtained for voids that form in the interior of the aluminum interconnects without surface contamination. $6.5 \times 10^{-6}\exp(-0.84\ \mathrm{eV}/kT)\ \mathrm{m}^2\ \mathrm{s}^{-1}$ is obtained for those voids that nucleate either at triple junctions or at the grain boundary-technical surface intersections, where the chemical impurities may act as trap centers for hopping vacancies.

Keywords: Electromigration; Interconnect failure; Damage mechanics; Void growth; Interfaces and surfaces; Diffusion; Thermodynamics

1. Introduction

Capillary-driven shape and microstructural evolution in solids continues to be a challenging theoretical problem in materials science. By drawing from elegant fundamental laws of physics, the field allows for the

* Corresponding author. Tel.: +90 312 210 2512; fax: +90 312 210 1267.
E-mail address: ogurtani@metu.edu.tr (T.O. Ogurtani).

0020-7683/$ - see front matter © 2004 Elsevier Ltd. All rights reserved.
doi:10.1016/j.ijsolstr.2004.11.013

exciting possibility of making quantitative prediction about the behavior of a diverse range of real materials such as sapphire or ice. The importance of this subject in materials science applications derives from the fundamental role played by surfaces and heterophase boundaries in physical and chemical processes in solids, in stability of structure and in properties of materials. Wetting, sintering, grain growth, grain boundary grooving, growth of thin films, and stability of multilayers are all examples of capillary driven shape and microstructural evolution.

In the early 1950s, a solid quantitative framework emerged in the classical works of Herring (1951), Von-Neumann (1952) and Mullins (1957). Their efforts relied strictly on principles of equilibrium thermodynamic, including Gibbs' description of interfaces and surfaces (Gibbs, 1948; Murr, 1975). The earliest analytical study was Mullins treatment of the grooving of a grain boundary (Mullins, 1957). Mullins ignored grain boundary diffusion and considered the junction to have the equilibrium capillarity configuration satisfying the Young relationship (Young, 1805). Chuang and Rice (1973), Pharr and Nix (1979), and also Huang et al. (2000) studied a very similar problem, namely the creep cavity growth on a grain boundary. They considered the coupling of surface diffusion along the interface separating the bulk phase from the cavity, and grain boundary diffusion driven by the gradient of the normal stress acting in the grain boundary. These two processes couple at the triple junction. The boundary conditions at the triple junction are continuity of chemical potential, conservation of mass, and the equilibrium capillarity configuration. In later, advanced numerical studies by Needleman and Rice (1980), Pan and Cocks (1994, 1995), Cocks (1994), and Kucherenko et al. (2000) and Averbuch et al. (2003a) similar thermostatic boundary conditions were employed at the triple junction in all cases. Most recently Khenner et al. (2001) have performed extensive numerical simulation of grain-boundary grooving by the level set method. However local thermodynamic equilibrium conditions are assumed at the groove roots. This assumption is also used by Ohring (1971) in analytical studies on electromigration damage in thin films.

Takahashi et al. (1991) studied void shrinkage utilizing two different numerical techniques, but relying on ad hoc models. One model restricts the dihedral angle θ to be given by the equilibrium force balance. In the other model, local equilibrium at the triple junction is ignored (i.e. free dihedral angle). The second model resulted in a bonding pressure exponent that is in agreement with the experimental observations, and a dihedral angle, which does not remain constant; instead, it changes as the net stress is increased at the bond-interface.

The steady state kinetics of triple junctions have also been investigated recently by Gottstein and Shvindlerman (2002) in their studies related to the grain growth of 2D polycrystals. They employed a modified version of the Von Neumann–Mullins relationship (Mullins, 2001) as a basis for the theoretical work. As a driving force for triple junction mobility, they assume a relationship, which may be valid only for symmetrically disposed dihedral angles having an equilibrium value of 60°. Liu et al. (2001) consider the similar problem of grain boundary crack growth in interconnects with an electric field. They also proposed that crack evolution is steady state and in which the angle of the crack apex is at equilibrium. They assert that the crack apex does not constitute a point source of entropy production, contradicting a key point in our theory of irreversible processes associated with the evolution dynamics of closed curved interfaces having triple junction singularities.

Increasingly, non-boundary tracking methods have been applied to simulate complex microstructural evolution, including Monte Carlo, cellular automata, and phase field methods (Mahadevan and Bradley, 1999). In the phase field approach the field variables are governed by semi-phenomenological equations of motion, e.g. the Cahn–Hilliard (Cahn and Hilliard, 1958) non-linear diffusion equation for the density field and the time-dependent Ginzburg–Landau (Landau and Lifshitz, 1980) equation for the long-range order parameter field. Kazaryan et al. (1999) generalized the phase field approach by allowing for rigid-body rotation during sintering and by further assuming that the triple junction velocity can be determined from the steady state requirement imposed at the grain boundary. Triple-junction motion has also been investigated by Cahn et al. (1996) using a coupled Allen-Cahn/Cahn–Hilliard (Novick-Cohen, 2000)

formulation and utilizing long time asymptotic analysis in which the requirement of the uniform displacement is still incorporated. They assume local physico-chemical equilibrium and continuity of chemical potentials at the triple junction. However, the more serious restriction associated with phase field method is the utilization of a symmetric "double well potential" for the free energy, which requires all interfacial energies to be equal. This restriction also hinders the particle growth process as admitted by the authors themselves.

In fracture mechanics, Chuang (1983) and notably Rice and Chuang (1981) seriously attempted to formulate the steady state crack growth via surface diffusion, by calculating the Irwin's energy-release rate that arises during the dissipative motion. Chuang tried to apply the bulk irreversible thermodynamics of continuum to this composite system by integrating non-additive entropy source term (Haase, 1969) and splitting total Helmholtz free energy into elastic and surface energies illegitimately. Nevertheless, they still kept the crack tip configuration (dihedral angles) in thermostatic equilibrium state with finite fictitious curvature. Chuang (1983) used Herring's (1951) surface chemical potential, which was modified by Rice and Chuang (1981) by replacing the standard chemical potential with the strain energy density. This modification was obtained by ambiguous and improper equilibrium considerations for the ordinary points by employing total Helmholtz free energy variance rather than the dissipation function inequality. This inequality approach is thermodynamically justified (Guggenheim, 1959) for composite macro-systems including surface phases not only for the reversible but also for the irreversible isothermal processes. Improper utilization of the thermodynamics resulted very serious and adverse sign conflict on the strain energy contribution to the generalized potentials and conjugated fluxes, which are responsible for the surface drift-diffusion, as well as the evaporation and condensation processes including solid-state phase transformations.

Up to now all theoretical studies related to the interfaces and surfaces which are reported and cited in the literature, rely strictly on the use of classical thermodynamics as a general tool for the macroscopic description of physico-chemical processes. Additionally some obscure modifications in the concept and usage of chemical potentials and the free energies have been included especially in the presence of externally imposed force fields (electrical, magnetic, etc.), without considering their original strictly mathematical definitions by Gibbs (1948). More serious limitations lie in the fact that the methods are based on reversible processes and true equilibrium states.

This paper focuses on the non-equilibrium thermodynamic treatment of interfacial triple junction singularities as a further supplement to our previously presented theory (Ogurtani and Oren, 2001) of irreversible processes applied to the shape evolution dynamics of closed surfaces and interfaces composed of ordinary points. By relying only on the fundamental postulates of linear irreversible thermodynamics for the bulk phases, as advocated by Prigogine (1961), Ogurtani (2000) has obtained a compact and rigorous analytical theory of a network of interfaces that are interconnected by triple junctions and embedded in bulk phases by utilizing the more realistic monolayer model of Verschaffelt (1936) and Guggenheim (1959) for the description of interfaces and surfaces. A brief summary of Ogurtani theory on the triple junction is reported recently by Oren and Ogurtani (2002) in connection with their computer simulation studies on the effect of various combinations of grain textures on the life time and the failure mechanisms of thin film interconnects with bamboo structures.

In Section 2, the linear thermodynamics of irreversible processes is introduced in the treatment of surfaces and bulk phases. A conventional macro-formulation for homogeneous and isotropic closed systems is used as a starting point for the local, micro-discrete formulation adopted in our work. The singular point associated with a triple junction is treated rigorously by using micro-discrete (straight) interfacial elements as a convenient mathematical tool and then passing to a continuum representation of the singular point by applying appropriate limit procedures. The generalized forces and conjugate fluxes associated with the triple junction are obtained in terms of the asymmetric dihedral angles and the specific Gibbs free energies related to the void surface layer and the grain boundary, respectively. The entropy production associated

with the virtual displacement of ordinary points, which is directly utilized without proof in our previous paper (Ogurtani and Oren, 2001), is also derived as a special or degenerate case of the singular point treatment. The contribution of the strain energy density to the generalized forces and the conjugated fluxes are analyzed rigorously by the first-order decomposition of the generalized Gibbs free energy density, which is an extension of the Lord Kelvin's and Gibbs's approaches to the stress tensor dependence of entropy density (Fung, 1965), at constant temperature and composition. This contribution is also compared with the other author's formulations of the so-called the surface chemical potential in terms of ad hoc combinations of elastic and surfaces energies, notably by Rice and Chuang (1981), and Suo and Wang (1994). The unjustified usage of the total Helmholtz free energy variance in the literature for the isothermal reversible processes in composite open systems is stressed, and its adverse consequences are demonstrated by a gedanken experiment.

In Section 3, a universal mathematical model for void shape evolution dynamics in the presence of void–grain boundary interactions is developed by introducing novel normalization and scaling procedures, which are entirely independent of specific material properties.

In Section 4, the results of our computer simulations are presented revealing a mechanism of trapping and detrapping of voids during intergranular motion under the action of capillary and electromigration forces. The results of the computer simulation studies performed on bamboo structures are summarized in terms of the mean time to failure MTTF, and upper and lower bonds associated with cathode failure of interconnects. Finally, those formulas are applied to the experimental MTTF data reported in the literature by various authors for materials having different microstructures and under different experimental conditions.

2. Micro-discrete open composite system with interfaces

2.1. Internal entropy production for discrete micro-elements

The term microscopic region refers to any small two or three-dimensional region containing a sufficiently large number of molecules so that microscopic fluctuations may be neglected, and so that all of intensive properties may be considered homogeneous. The composite system considered here has at least two physico-chemically distinct domains separated by thin interphase layers. The layers interact by exchange of matter and energy and are completely open to the surroundings through moving or immobile boundaries. For the specific case of a triple junction, the system is an open composite system. It is composed of two bulk phases, namely the interconnect material and the embedded void, and two surface phases, the interfacial layer between the void and the bulk region and the grain boundary separating two different grains of the interconnect.

In this theory, the general approach used by Guggenheim (1959) and van der Waals and Baker (1928) is adopted to treat the interface between any two phases or domains. This approach assumes the interface to be an autonomous, finite but thin layer across which the physical properties and/or the structures vary continuously from those of the interior of one phase to those of the interior of the other. The temperature, entropy, free energy, and composition are defined as in the homogeneous bulk phases. The only functions that require special consideration are the pressure P and the interfacial (surface) tension γ. In the absence of long range forces, *the total reversible work* done on a flat micro-surface phase, which is indicated by Δ finite element operator, by variations in volume $d\Delta V_\sigma$, and in area $d\Delta A_\sigma$ due to stretching while maintaining material content unaltered, is given by the following well known expression: $\delta\Delta w = -\bar{P}_\sigma d\Delta V_\sigma + \gamma d\Delta A_\sigma$. It is assumed that the principal stress component of the axisymmetric 3-D interfacial layer stress tensor, $\bar{\bar{\sigma}}$, directed along the surface normal $P_z = \hat{z}\cdot\bar{\bar{\sigma}}\cdot\hat{z}$, is quasi-homogenous in the micro-layer, and the other two transverse components denoted by $\hat{t}_\perp\cdot[\bar{\bar{I}}P_z - \bar{\bar{Q}}]\cdot\hat{t}_\perp$ are equal (rotational symmetry) but heterogeneous along the surface

normal $\hat{z}$. $\bar{P}_\sigma = \frac{1}{h}\int_0^h P_z \,\mathrm{d}z$ is the mean pressure in the layer, and γ is called the interfacial tension or the surface tension in the case of liquids. The value of γ and its location of the surface within which it is defined can be uniquely determined by the knowledge of the transverse components of the stress tensor (Buff, 1955; Ono and Kondo, 1960; Laplace, 1806). Its value is given by $\gamma = \int_0^{h_\sigma} \hat{t}\cdot\bar{\bar{Q}}\cdot\hat{t}\,\mathrm{d}z$, where $\bar{\bar{Q}} = \bar{\bar{\sigma}} - \hat{z}\cdot\bar{\bar{\sigma}}\cdot\hat{z}\bar{\bar{I}}$ is a 2-D reducible tensor acting only on the surface tangent planes, and it is isotropic in the present case because of the axisymmetric stress system. The integration is performed along the surface normal and h_σ is the thickness of the surface layer. These reducible 2-D dyadics may be also called 'the generalized surface stress tensor' by lifting the rotational symmetry on $\bar{\bar{\sigma}}$, but keeping $\hat{z}$ as a principal axis in the layer, in order to have an additional contribution to the reversible work by interacting with the shear part of the surface deformation tensor. This possibility, results a new definition of the interfacial tension $\gamma_{\alpha,\beta} = \int_0^h t_\alpha\cdot\bar{\bar{Q}}\cdot t_\beta\,\mathrm{d}z$, which is tensorial quantity acting on the arbitrary plane deformation of the surface layer $\mathrm{d}\Delta A_{\alpha,\beta} = \bar{\bar{\sum}}_{\alpha,\beta} d\Delta A,\ (\alpha,\beta \Leftarrow 1,2)$ while keeping its volume constant. Here $\bar{\bar{\Sigma}}$ is the plane distortion tensor in 2-D space. This results in a new generalization of the reversible work done on the interfacial layer, which is given by $\bar{\bar{\gamma}}\otimes\bar{\bar{\Sigma}}d\Delta A_\sigma$. The reversible work expression should be modified as $\delta\Delta w = -\bar{P}_\sigma d\Delta V_\sigma + \bar{\bar{\gamma}}\otimes\bar{\bar{\Sigma}}d\Delta A_\sigma$ in order to take full account for the shear components of the surface stress tensor.

In the conventional theory of irreversible processes (Prigogine, 1961), it has been postulated that the Gibbs formula, which is derived for reversible changes, is also valid for irreversible processes. However in the present formulation, it is tacitly postulated that the differential form of the Helmholtz free energy defined at equilibrium may be extended to treat irreversible changes. Mathematically, this assumption is exactly equivalent to the Gibbs formula used extensively in the standard treatment.

The local anisotropic properties of the medium are automatically embedded in the intensive variables, which are characterized by second order tensors or dyadics depending on the orientation of the surface normal. Hence the Helmholtz free energy for an open surface phase of micro-extent and embedded in an isotropic media may be written as,

$$\mathrm{d}\Delta F_\sigma = -\Delta S_\sigma dT_\sigma - \bar{P}_\sigma d\Delta V_\sigma + \bar{\bar{y}}\otimes\bar{\bar{\Sigma}}d\Delta A_\sigma + \sum_i \mu_\sigma^i d\Delta n_\sigma^i - \sum_j \Delta A_\sigma^j d\xi_\sigma^j, \tag{1}$$

where ΔS_σ denotes the entropy, μ_σ^i denotes the chemical potential, Δn_σ^i is the number of ith chemical species in the micro-element, $d\xi_\sigma^j$ is the extent of the homogeneous jth chemical reaction taking place in the phase under consideration, and ΔA_σ^j is the affinity of the homogeneous jth chemical reaction as defined by Donder and van Rysselberghe (1936).

In Eq. (1) it is assumed that in a single phase only homogeneous chemical reactions take place and phase transitions occurring at mobile boundaries are not considered in the last term. The change in the Helmholtz free energy due to the passage of substance i from the phase to the surroundings is included in the fourth term of Eq. (1) (frozen chemical reactions). Therefore, in the case of a closed system, one should subtract only the term $\sum_i \mu_\sigma^i d\Delta n_\sigma^i$, which is closely related to the direct exchange of matter with the surroundings. For a bulk phase one may write the expression for a micro-system as,

$$d\Delta F_\mathrm{b} = -\Delta S_\mathrm{b} dT_\mathrm{b} - P_\mathrm{b} d\Delta V_\mathrm{b} + \sum_i \mu_\mathrm{b}^i d\Delta n_\mathrm{b}^i - \sum_j \Delta A_\mathrm{b}^j d\xi_\mathrm{b}^j. \tag{2}$$

In the case of a composite system, the total Helmholtz free energy differential can be easily written down from Eqs. (1) and (2) since extensive thermodynamic quantities are additive.

The entropy of any closed or open system can change by the interchange of entropy with its surroundings, external interactions, $d\Delta S_\mathrm{ex}$, and by the internal entropy production (IEP) inside the system, $d\Delta S_\mathrm{in}$. Symbolically, one may write this as: $d\Delta S = d\Delta S_\mathrm{in} + d\Delta S_\mathrm{ex}$. The entropy increase $d\Delta S_\mathrm{in}$ due to changes taking place inside the system is positive for all natural or irreversible changes, vanishes for all reversible changes and is never negative.

Generalizing the first law of thermodynamics for any infinitesimal change associated with an open system in which energy and matter exchange occurs between the system and its surroundings, gives

$$\delta\Delta\Phi = d\Delta U - \delta\Delta w = d(\Delta F + T\Delta S) - \delta\Delta w. \tag{3}$$

$\delta\Delta\Phi$is the energy received by the system due to heat and matter transfer processes from the surroundings, $d\Delta U$ is internal energy change, and $\delta\Delta w$ is the reversible work done on the system which is equal to $-Pd\Delta V$ (bulk phase) or $-(Pd\Delta V - \gamma d\Delta A)$ (surface phase).

Globally, for a composite system having discontinuous phases, the total IEP due to irreversible processes should include contributions due to the transport of heat and chemical species among the various phases of the system. Hence, from Eqs. (1), or ((2) and (3), by adding entropy changes, and then splitting the results (Prigogine, 1961) the following relationship for an ensemble of multi-phase micro-element system, consisting of interconnected two open phase sub-systems with interfaces, is obtained.

$$\frac{d\Delta S_{\text{in}}}{\delta t} = -\sum_{i,k}\frac{\mu_k^i}{T_k}\frac{d\Delta n_k^i}{\delta t} + \sum_k \frac{1}{T_k}\frac{\delta\Delta\Omega_k}{\delta t} + \sum_{j,k}\frac{\Delta A_k^j}{T_k}\frac{d\xi_k^j}{\delta t}. \tag{4}$$

Eq. (4) allows for homogeneous chemical reactions occurring in the different phases of the (global) open system. Index k refers to summation taken over (bulk or surface) phases, and indices i and j refers to summation over chemical species or reactions that occurring in the kth phase. $\delta\Delta\Omega_k$ is the amount of energy transported to the kth individual phase from the other phases present in the system due to heat or mass transfer. The first term in Eq. (4) represents an additional contribution to the IEP in the composite system due to internal entropy flow associated with the transfer of chemical species from one sub-domain to another sub-domain. Note that the second term in the entropy production for a composite system drops out for those sub-domains having the same temperature.

The IEP is not an additive property of a thermodynamic system composed of interacting open sub-systems unless the whole system is in a state of complete physico-chemical equilibrium (Haase, 1969). Therefore, in order to calculate the global IEP for the whole system composed of a set of discrete but interconnected micro-elements and the matrix in which the micro-elements are embedded, the rate of entropy flow (REF) should also be formulated by utilizing appropriate summation or integration operations as demonstrated by Ogurtani and Oren (2001).

The REF from the surroundings into an open composite system may be written

$$\frac{d\Delta S_{\text{ex}}}{\delta t} = -\sum_{i,k}\frac{\mu_k^i}{T_k}\frac{d\Delta n_{k\leftrightarrow s}^i}{\delta t} + \sum_k \frac{1}{T_k}\frac{\delta\Delta\Omega_{k\leftrightarrow s}}{\delta t} \quad \text{(Open composite micro-system)}, \tag{5}$$

where the subscript $_{k\leftrightarrow s}$ indicates that matter and energy exchange takes place between the phases of the system, k, and the surroundings, s. Here, $\delta\Delta\Omega_{k\leftrightarrow s}/\delta t$ and $d\Delta n_{k\leftrightarrow s}^i/\delta t = J_{k,s}^i$ are the flow rate of energy and flux of chemical species i to the domain k of the composite open micro-system from the surroundings, through heat and matter exchange processes respectively.

2.2. Internal entropy productions associated with the virtual displacements of the triple junction and the ordinary points

Here, the irreversible thermodynamic theory of the evolution dynamics of ordinary points along a void surface and the displacement kinetics of a triple junction is given. The relevant parts are summarized in our recent publications (Ogurtani and Oren, 2001; Oren and Ogurtani, 2002). However in the first paper, the local entropy production or the entropy source term associated with the virtual displacement of an ordinary point is referred to unpublished work of Ogurtani (2000). In this section we will show that it may be derived as a special case of a triple junction singularity by relaxing certain geometric constraints on the system in the presence of a grain boundary.

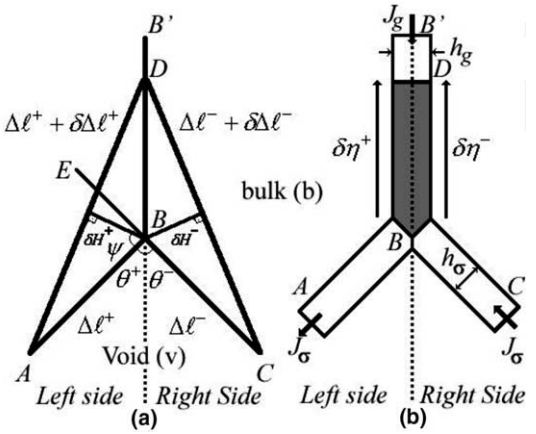

Fig. 1. Longitudinal displacement of a triple junction along the grain boundary. (a) Triple junction macrostructure. (b) Triple junction microstructure. BB' is the grain boundary, ABC and ADC are the initial and the displaced positions respectively of the void interfacial layer, and $\delta\eta$ is the longitudinal virtual displacement of the triple junction along the grain boundary.

It is assumed that the whole system is in thermal equilibrium and no in situ chemical reaction occurs. The only transition is the phase transformation occurring at the void interfacial layer and in the grain boundary region. This last consideration has been omitted in the literature (Rice and Chuang, 1981). But it is crucial to the development of the entropy point source term. In the present theory the sampling domain is a very small, discrete and open composite micro-system. The domain will eventually be localized into a singular point situated in the immediate neighborhood of the junction as illustrated in Fig. 1. The composite micro-system is also connected to the neighboring micro-discrete elements by nodes where the exchange or the flow of matter contributes to the REF but not to the IEP.

First the individual IEP due to a small but finite virtual advancement of a triple junction along the grain boundary is calculated by assuming that chemical potentials do not depend on the orientation of the surface normal. The sampling region at the triple junction is divided into two sub-domains by a line, which separates the grain boundary region into two symmetrical parts. However, at a later stage in the derivation, the IEP associated with the virtual displacement of the triple junction along directions parallel and perpendicular to the grain boundary is also calculated by lifting the constraints on triple junction motion.

The internal entropy variation for the left hand side sub-system when the triple junction moves a distance $\delta\eta^+$ along the grain boundary is calculated. The following variational relationships among various quantities are deduced from Fig. 1, by using simple geometric arguments and assuming that $\Delta\ell^+ \gg \delta\eta^+$ and $\Delta\ell^- \gg \delta\eta^-$. The variational relationships are:

$$\delta\Delta\ell^+ = \cos\theta^+\delta\eta^+, \quad \delta H^+ = \sin\theta^+\delta\eta^+, \tag{6}$$

$$\delta\Delta n_{\mathrm{b}}^+ = -\frac{1}{2\Omega_{\mathrm{b}}}\Delta\ell^+\sin\theta^+\delta\eta^+, \quad \delta\Delta n_{\mathrm{v}}^+ = \frac{1}{2\Omega_{\mathrm{v}}}\Delta\ell^+\sin\theta^+\delta\eta^+, \tag{7}$$

$$\delta\Delta n_\sigma^+ = \frac{h_\sigma}{\Omega_\sigma}\cos\theta^+\delta\eta^+, \quad \text{and} \quad \delta\Delta n_{\mathrm{g}}^+ = -\frac{h_{\mathrm{g}}}{2\Omega_{\mathrm{g}}}\delta\eta^+, \tag{8}$$

where Ω_σ, Ω_g, Ω_{b} and Ω_{v} are the mean atomic specific volumes associated with the void surface layer, the grain boundary, the bulk and void phases, respectively. $\Delta\ell^+$ and $\Delta\ell^-$ denote segment lengths of the void surface layer adjacent to the right and left hand sides of the triple junction, respectively. h_σ and h_{g} are the thicknesses of the surface layer and the grain boundary region and are assumed to be invariant.

$\delta\Delta n_{\rm v}^{+}(\delta\Delta n_{\rm b}^{+})$ is the number of atoms gained in the reaction zone associated with the void interfacial layer (bulk interfacial layer) while the transformation processes are taking place during the virtual displacement of the interfacial layer. $\delta\Delta n_{\rm g}^{+}$ is the total number of atoms misplaced by one-half of the grain boundary during triple junction motion. Similarly, $\delta\Delta n_{\sigma}^{+}$ is equal to the net atomic gain by the interfacial layer (denoted by σ) due to enlargement (extension without stretching) of that layer during the displacement operation. δ and Δ are variational and micro-discretization operators, respectively. Eventually, by using a set of novel limiting procedures these quantities will be replaced by exact differentials, and zeros that correspond to an infinitesimal volume or to the singularity associated with the triple junction. One can obtain exactly similar expressions for the other side of the triple junction; these values will be denoted by a negative sign superscript in the formulas. The following identities are employed in our formulas: $\Gamma_{\sigma} = h_{\sigma}/\Omega_{\sigma}$ and $\Gamma_{\rm g} = h_{\rm g}/\Omega_{\rm g}$. They correspond to the specific mean atomic densities associated with the void surface layer and with the grain boundary, respectively.

By applying the first term of Eq. (4), which is the only term that does not vanish on the left and right sides of the sub-composite systems, the IEP generation can be calculated for any arbitrary virtual displacement of the triple junction along the grain boundary. Also, one should recall that in the case of a multi-component system, the variation in the number of atomic species could easily be obtained by simply multiplying the total atomic number variations by the respective atomic fractions x_j^i. As an example, the number of chemical species in the left hand side bulk phase due to the virtual displacement may be given by

$$\delta\Delta n_{\rm b}^{i+} = x_{\rm b}^{i}\delta\Delta n_{\rm b}^{+} = \frac{x_{\rm b}^{i}}{2\Omega_{\rm b}}\Delta\ell^{+}\sin\theta^{+}\delta\eta^{+}. \tag{9}$$

One can then rigorously write down the rate of entropy production due to triple junction virtual displacement for the left as well as for the right hand side domains using Eqs. (4), (6)–(9). In the case of the left hand side the REP is denoted by the following formula:

$$\frac{\delta\Delta S_{\rm in}^{+}}{\delta t} = \frac{1}{T}\left\{\sum_i\left(\frac{x_{\rm b}^{i+}}{\Omega_{\rm b}}\mu_{\rm b}^{i+} - \frac{x_{\rm v}^{i+}}{\Omega_{\rm v}}\mu_{\rm v}^{i+}\right)\frac{1}{2}\Delta\ell^{+}\sin\theta^{+} + \frac{\Gamma_{\rm g}}{2}\sum_i x_{\rm g}^{i}\mu_{\rm g}^{i} - \Gamma_{\sigma}\cos\theta^{+}\sum_i x_{\sigma}^{i+}\mu_{\sigma}^{i+}\right\}\frac{\delta\eta^{+}}{\delta t}. \tag{10}$$

In above relationship, we have employed a subscript '+' above both the atomic fractions and the chemical potentials of the surface phase in order to indicate explicitly that these quantities may depend upon the local surface orientation. One should also recall that for multi-component surface phases, the quantities $\sum\Gamma_{\sigma}^{i}\mu_{\sigma}^{i}$, and $\sum\Gamma_{\rm g}^{i}\mu_{\rm g}^{i}$ are equal to the specific Gibbs free energy densities associated with the void surface layer, and the grain boundary, respectively. These quantities will be denoted by g_{σ} and $g_{\rm g}$. Here, $\Gamma_{\sigma}^{i} = \Gamma_{\sigma}x_{\sigma}^{i}$, and $\Gamma_{\rm g}^{i} = \Gamma_{\rm g}x_{\rm g}^{i}$ are defined as the specific surface concentrations of chemical species in the surface layer, and in the grain boundary, respectively.

The terms appearing in the first group on the right side of Eq. (10), e.g. $\sum x_{\rm b}^{i}\mu_{\rm b}^{i}/\Omega_{\rm b}$ and $\sum x_{\rm v}^{i}\mu_{\rm v}^{i}/\Omega_{\rm v}$, are the volumetric Gibbs free energy densities associated with the bulk phase and the void region. These quantities are denoted by $\breve{g}_{\rm b}$ and $\breve{g}_{\rm v}$, and each has unique instantaneous compositions at points adjacent to the hypothetical geometric boundaries of the interfacial layer (reaction fronts or zones). Furthermore, these quantities are related to the specific Gibbs free energy densities by the relationship: $g_{\sigma} = h_{\sigma}\breve{g}_{\sigma}$.

Dividing both sides by δt, and then taking consecutively the limits, $\delta t \to 0$, and $\Delta\ell \to 0$, the following differential equations associated with the virtual displacement of the left and right sides of the triple junction singularity, representing IEP are obtained:

$$\lim_{\substack{\delta t\to 0\\ \Delta\ell\to 0}}\frac{\delta\Delta S_{\rm in}^{+}}{\delta t} = \frac{{\rm d}\Delta\hat{S}_{\rm in}^{+}}{{\rm d}t} = \frac{1}{T}\left(\frac{1}{2}g_{\rm g} - g_{\sigma}^{+}\cos\theta^{+}\right)\frac{{\rm d}\eta^{+}}{{\rm d}t} \quad \left({\rm J\,K^{-1}\,m^{-1}\,s^{-1}}\right) \tag{11}$$

and

$$\lim_{\substack{\delta t\to 0\\ \Delta\ell\to 0}} \frac{\delta\Delta S^{-}_{\rm in}}{\delta t} = \frac{{\rm d}\Delta\hat{S}^{-}_{\rm in}}{{\rm d}t} = \frac{1}{T}\left(\frac{1}{2}g_{\rm g} - g^{-}_{\sigma}\cos\theta^{-}\right)\frac{{\rm d}\eta^{-}}{{\rm d}t} \quad \left({\rm J\,K^{-1}\,m^{-1}\,s^{-1}}\right). \tag{12}$$

On the left sides of above expressions, the hat symbol $\hat{}$ indicates that these entropy production terms are line sources in three-dimensional space. The voids are treated as cylinders. Finally, we can choose a local set of discrete micro-elements in the vicinity of the triple junction, which includes both domains mentioned previously. The entropy production for the combined system can be calculated using the above arguments for the virtual displacement of the triple junction along the grain boundary. The result is:

$$\begin{aligned}\frac{\delta\Delta S^{g\sigma}_{\rm in}}{\delta t} &= \frac{\delta\Delta S^{+}_{\rm in}}{\delta t} + \frac{\delta\Delta S^{-}_{\rm in}}{\delta t}\\ &= \frac{1}{T}\left\{-\frac{1}{2}\left(\breve{g}^{+}_{\rm vb}\Delta\ell^{+}\sin\theta^{+} + \breve{g}^{-}_{\rm vb}\Delta\ell^{-}\sin\theta^{-}\right) + \left[g_{\rm g} - \left(g^{+}_{\sigma}\cos\theta^{+} + g^{-}_{\sigma}\cos\theta^{-}\right)\right]\right\}\frac{\delta\eta_{\rm g}}{\delta t} \geqslant 0.\end{aligned} \tag{13}$$

Eq. (13) yields the IEP due to the longitudinal displacement of the triple junction along the grain boundary. Then applying the consecutive limiting procedures previously described gives:

$$\frac{{\rm d}\hat{S}^{g\sigma}_{\rm in}}{{\rm d}t} = \frac{1}{T}\left[g_{\rm g} - \left(g^{+}_{\sigma}\cos\theta^{+} + g^{-}_{\sigma}\cos\theta^{-}\right)\right]\frac{{\rm d}\eta_{\rm g}}{{\rm d}t} \geqslant 0, \tag{14}$$

where $\breve{g}_{\rm vb} = (\breve{g}_{\rm v} - \breve{g}_{\rm b})$ is the volumetric Gibbs Free energy density of transformation (GFEDoT) associated with the transformation of bulk phase into *realistic void* phase. The realistic void phase is a solid or fluid phase containing chemical species even though they may be present only in trace amount. In the case of thermostatic equilibrium between a void phase and an adjacent bulk phase, the GFEDoT vanishes, if the reaction front is flat. The connection between the GFEDoT and the Specific Gibbs Free Energy of transformation $g_{\rm vb}$ between the parent phase and void phase is $g_{\rm vb} = \breve{g}_{\rm vb}h_{\sigma}$. (Note that for evaporation of bulk or growth of void region, $g_{\rm vb} < 0$.)

It should also be mentioned that the IEP density associated with the virtual displacement of an ordinary point along the direction normal to the void surface could also be rigorously deduced from Eq. (13). This is accomplished by omitting the contribution due to the grain boundary interaction, and also recognizing that the displacement motion of the curved interface takes place along the local surface normal vector. Since the right and the left hand segments around a selected ordinary point can be chosen arbitrarily, we may take them equal in length. This automatically results in identical angles between the surface normal and the right and the left segments at the emerging point. Applying the sequential limiting procedure such that $\Delta\ell \to 0$ and $\delta t \to 0$, then the following rigorous continuum relationship may be obtained,

$$\kappa = \lim_{\Delta\ell\to 0}\frac{\cos\theta}{\Delta\ell/2}, \tag{15}$$

where the definition of the local radius of curvature, $\rho = \kappa^{-1}$, has been used.

Similarly $\lim_{\Delta\ell\to 0}\theta = \pi/2$. Hence, using the limits given in Eq. (13), the following expression for the internal entropy production density (the entropy source term) associated with ordinary points is calculated:

$$\frac{{\rm d}\hat{S}_{\rm in}}{{\rm d}t} = -\frac{1}{T}\left(\breve{g}_{\rm vb} + g_{\sigma}\kappa\right)\frac{{\rm d}\eta}{{\rm d}t} \geqslant 0 \quad \left({\rm J\,K^{-1}\,m^{-2}\,s^{-1}}\right). \tag{16}$$

Freedom exists in the choice of fluxes and forces, because the entropy production can be split in several ways into fluxes and forces (De Groot, 1951). The set of forces and fluxes that is employed in our previous paper (Ogurtani and Oren, 2001) in connection with ordinary points along the void surface layer is based on thermodynamic considerations. However, the interpretation of these forces is rather abstract, and they

may be also referred to as affinities in the field of irreversible thermodynamics. On the other hand, a second approach can be developed in terms of *a drag force* and a *velocity*. This interpretation is straightforward, but its validity is restricted to systems that are in complete thermal equilibrium, and so all processes are isothermal. Since thermal equilibrium has been discussed in this system, we may use the concept of the power dissipation function (Haase, 1969) to interpret the triple junction singularity. This concept was further generalized by postulating the power input function for time and space dependent external excitations and extensively used in a general formulation of internal friction and in kink (solitons) dynamics by Ogurtani and Seeger (1985, 1987) and Ogurtani (1989). The power dissipation function is simply given by the product of the internal entropy production with the temperature in an isothermal system. In the present case it is identically equal to product of the driving force with the velocity:

$$T\frac{\mathrm{d}\hat{S}^{\pm}_{\mathrm{in}}}{\mathrm{d}t}=\widehat{F}^{\pm}\frac{\mathrm{d}\eta^{\pm}}{\mathrm{d}t}\geqslant 0\quad\left(\mathrm{J\,m^{-1}\,s^{-1}}\right). \tag{17}$$

By comparing this expression with Eq. (11) the generalized force on the left side is identified as:

$$\widehat{F}^{+}=\left(\frac{g_{\mathrm{g}}}{2}-g^{+}_{\sigma}\cos\theta^{+}\right)\ \left(\mathrm{N\,m^{-1}}\right). \tag{18}$$

Similarly, by comparing Eq. (17) with Eq. (12), then

$$\widehat{F}^{-}=\left(\frac{g_{\mathrm{g}}}{2}-g^{-}_{\sigma}\cos\theta^{-}\right)\quad\left(\mathrm{N\,m^{-1}}\right). \tag{19}$$

These generalized forces are associated with net material flow during triple junction longitudinal displacement along the grain boundary without distinction between intrinsic fluxes associated with the individual chemical species. Units are per unit length because in our formulation of the IEP, a sample of unit length in thickness is chosen, and the void surface is assumed to be an arbitrary cylindrical shape. In the phenomenological relationship between velocity and force, one may prefer to use the force acting on a single atomic particle. In this case the above expressions for the generalized forces should be multiplied by an atomic length, d_{a}, which may be the interatomic distance along the sample thickness. Hence, the connection between the triple junction velocity and the generalized atomic force can now be written by introducing the phenomenological mobility coefficient $\mathfrak{R}^{\mathrm{long}}/kT$,

$$\frac{\mathrm{d}\eta^{+}}{\mathrm{d}t}=\frac{\mathfrak{R}^{\mathrm{long}}d_{\mathrm{a}}}{kT}\left(\frac{g_{\mathrm{g}}}{2}-g^{+}_{\sigma}\cos\theta^{+}\right) \tag{20}$$

and

$$\frac{\mathrm{d}\eta^{-}}{\mathrm{d}t}=\frac{\mathfrak{R}^{\mathrm{long}}d_{\mathrm{a}}}{kT}\left(\frac{g_{\mathrm{g}}}{2}-g^{-}_{\sigma}\cos\theta^{-}\right). \tag{21}$$

The same mobilities are employed for both sides of the triple junction. The atomic fluxes coming from the triple junction towards either side of the void surface layer can be determined. These are given by the number of atoms present in a volume swept by the motion of the triple junction along the grain boundary per unit time, plus the incoming grain boundary atomic flux $\hat{J}_{\mathrm{g}}(\#\mathrm{m^{-1}\,s^{-1}})$ associated with the long-range drift-diffusion. Since the velocity of the triple junction is proportional to the net flux accumulated or depleted at the junction, then

$$\frac{\mathrm{d}\eta^{+}_{\mathrm{g}}}{\mathrm{d}t}=\frac{2}{\Gamma_{\mathrm{g}}}\left(\hat{J}^{+}_{\sigma}-\hat{J}_{\mathrm{g}}/2\right)\quad\text{and}\quad\frac{\mathrm{d}\eta^{-}_{\mathrm{g}}}{\mathrm{d}t}=-\frac{2}{\Gamma_{\mathrm{g}}}\left(\hat{J}^{-}_{\sigma}+\hat{J}_{\mathrm{g}}/2\right). \tag{22}$$

Combining these expressions with Eqs. (20) and (21) for the triple junction velocities, gives the following generalized conjugate fluxes:

$$\widehat{J}_{\sigma}^{+} = \Gamma_{\mathrm{g}} \frac{\Re^{\mathrm{long}} d_{\mathrm{a}}}{2kT} g_{\sigma}^{+} \left(\lambda^{+} - \cos\theta^{+}\right) + \hat{J}_{\mathrm{g}}/2 \tag{23}$$

and

$$\widehat{J}_{\sigma}^{-} = -\Gamma_{\mathrm{g}} \frac{\Re^{\mathrm{long}} d_{\mathrm{a}}}{2kT} g_{\sigma}^{-} (\lambda^{-} - \cos\theta^{-}) - \hat{J}_{\mathrm{g}}/2. \tag{24}$$

The sample thickness is chosen to be unit length; splitting the grain boundary diffusion flux into equal components separates the right and left sub-domains. The expression for the velocity of the triple junction is determined directly from Eq. (14), or by applying the law of conservation of species to the displacement motion of triple junction, and substituting Eqs. (23) and (24) for the out-going fluxes from the transformation front:

$$v_{\mathrm{g}}^{\mathrm{long}} = \frac{\mathrm{d}\eta_{\mathrm{g}}}{\mathrm{d}t} = \left(\widehat{J}^{+} - \widehat{J}^{-} - \widehat{J}_{\mathrm{g}}\right) \frac{1}{\Gamma_{\mathrm{g}}} = \frac{\Re^{\mathrm{long}} d_{\mathrm{a}}}{2kT} \left[g_{\mathrm{g}} - \left(g_{\sigma}^{+} \cos\theta^{+} + g_{\sigma}^{-} \cos\theta^{-}\right)\right]. \tag{25}$$

In above flux relations, λ^{-} and λ^{+} may be assumed to be constant. In the case of isotropic surface phase properties λ^{-} and λ^{+} are equal. λ^{-} and λ^{+} are called wetting parameters and are given by: $\lambda^{-} = g_{\mathrm{g}}/(2g_{\sigma}^{-})$ and $\lambda^{+} = g_{\mathrm{g}}/(2g_{\sigma}^{+})$. The specific Gibbs free energy of the void surface layer may depend on the orientation of the local surface normal if the surface tension γ is anisotropic and/or if the specific Helmholtz free energy represents a crystalline solid (Defay et al., 1966).

In above expressions, a phenomenological mobility coefficient has been introduced and denoted by $\Re^{\mathrm{long}}$. The coefficient may be identified as a reaction rate constant associated with the phase transformation denoted symbolically by $\sigma \Longleftrightarrow gb$. For the present case, it refers to a transformation, which takes place continuously and reciprocally between two surface phases, namely, the interfacial void surface layer and the grain boundary region at the triple junction. This phenomenological mobility is strongly temperature dependent, and may be formulated according to the activated complex theory of chemical reaction rates (Yeremin, 1979) as follows:

$$\Re^{\mathrm{long}} = \left(\frac{kT}{h}\right) \exp\left(-\frac{\Delta G_{\sigma,\mathrm{g}}^{*}}{kT}\right). \tag{26}$$

In Eq. (26) $\Delta G_{\sigma,\mathrm{g}}^{*}$ is the Gibbs free energy of activation for the transformation of surface phase into the grain boundary phase or vice versa. Thermostatic equilibrium is established when the dihedral angles have reached those values which make the generalized forces given in Eqs. (18) and (19) identically zero, under the constraint of no lateral motion of the triple junction. In the case of isotropic specific Gibbs free energies $(g_{\sigma}^{+} = g_{\sigma}^{-} = g_{\sigma})$ Eq. (25) may be written:

$$v_{\mathrm{g}}^{\mathrm{long}} = \frac{\Re^{\mathrm{long}} d_{\mathrm{a}} g_{\sigma}}{2kT} \left[2\lambda - \left(\cos\theta^{+} + \cos\theta^{-}\right)\right] \quad \left(\mathrm{m\ s^{-1}}\right), \tag{27}$$

where $\lambda = g_{\mathrm{g}}/(2g_{\sigma})$. It follows that the internal entropy production associated with the transverse virtual displacement of the triple junction perpendicular to the grain boundary is given by

$$\frac{\delta \Delta S_{\mathrm{in}}^{\mathrm{trans}}}{\delta t} = -\frac{1}{T}\left\{\frac{1}{2}\left(\breve{g}_{\mathrm{vb}}^{+} \Delta\ell^{+} \cos\theta^{+} - \breve{g}_{\mathrm{vb}}^{-} \Delta\ell^{-} \cos\theta^{-}\right) + g_{\sigma}^{+} \sin\theta^{+} - g_{\sigma}^{-} \sin\theta^{-}\right\} \frac{\delta\eta^{\mathrm{trans}}}{\delta t} \geqslant 0. \tag{28}$$

By imposing the limiting procedures $\Delta t \to 0$ followed by $\Delta\ell^{\pm} \to 0$ an expression for the triple junction singularity, and hence, the internal entropy production for the transverse motion of the triple junction along the designated positive direction is determined;

$$\frac{\mathrm{d}\hat{S}_{\mathrm{in}}^{\mathrm{trans}}}{\mathrm{d}t} = -\frac{1}{T}\left(g_{\sigma}^{+} \sin\theta^{+} - g_{\sigma}^{-} \sin\theta^{-}\right) \frac{\mathrm{d}\eta^{\mathrm{trans}}}{\mathrm{d}t} \geqslant 0. \tag{29}$$

Since it is assumed that the composite system is in thermal equilibrium, according to Eq. (29) the component of the dissipative force acting along a direction perpendicular to the grain boundary may be given by

$$F^{\text{trans}} = g_\sigma^- \sin\theta^- - g_\sigma^+ \sin\theta^+ \quad \left(\text{N m}^{-1}\right). \tag{30}$$

This relationship together with Eq. (25) shows that a triple junction (without constraint) can be in complete physico-chemical equilibrium if and only if the specific interfacial Gibbs free energies associated with the grain boundary and with both sides of the void surface layer satisfy a *vectorial summation rule*, $\vec{g}_{\text{g}} + \vec{g}_\sigma^+ + \vec{g}_\sigma^- = 0$. The Young formula (Young, 1805) is a similar vectorial relationship between the surface tensions γ associated with the intersecting interfaces in order that mechanical equilibrium exists at the triple junction.

These results have impact on more general cases of virtual transverse triple junction motion. If one considers a more general problem where the grain boundary migration occurs as a result of thermally activated processes, the transverse component of the triple junction velocity according to Eq. (30) may be given by the following expression:

$$v_{\text{g}}^{\text{trans}} = \frac{\mathfrak{R}_{\text{g}}^{\text{trans}}}{kT} d_{\text{a}} \left(g_\sigma^- \sin\theta^- - g_\sigma^+ \sin\theta^+\right) \quad \left(\text{m s}^{-1}\right), \tag{31}$$

where d_{a} is the interatomic distance and $\mathfrak{R}_{\text{g}}^{\text{trans}}/kT$ is the transverse triple junction migration mobility. The latter is a phenomenological coefficient that is a function of the temperature of the system.

In the case in which lateral constraint is imposed on grain boundary motion, the generalized lateral force now generates particle flow throughout the triple junction region along the void interfacial layer, since, orientations of the neighboring left and right micro-elements need to adjust in order to establish a thermostatic equilibrium configuration. The conjugate particle flux (transverse flow) associated with this force can be written:

$$\hat{J}_\sigma^{\text{trans}} = -Sign(\psi)\Gamma_{\text{g}} \frac{\mathfrak{R}_{\text{g}}^{\text{trans}}}{kT} d_{\text{a}} \left(g_\sigma^- \sin\theta^- - g_\sigma^+ \sin\theta^+\right) \quad \left(\#\text{m}^{-1}\,\text{s}^{-1}\right). \tag{32}$$

The angle ψ denotes the amount of rotation of the micro-elements adjoint to the triple junction in the counter-clockwise direction, and Sign is the usual sign function.

2.3. Global internal entropy production associated with the virtual displacement of an interface interacting with grain boundaries

The global IEP (GIEP) is associated with the arbitrary virtual displacement $\mathrm{d}\eta/\mathrm{d}t$ of an interfacial loop of finite thickness separating a second phase particle v (realistic void) from the bulk multi-component matrix. In deriving the GIEP, the rate of local entropy density change along the curved interphase boundary must be integrated in order to obtain the desired relationship between the generalized forces and conjugate fluxes. The rate of local entropy density change is the only extensive, integrable quantity. Therefore, not only the local internal entropy production (source term) given by Eq. (16), but also the external entropy flow term needs to be evaluated for the virtual displacement of an interface. For isothermal processes the linear combination of these two terms is given by

$$\frac{\partial \hat{S}}{\partial t} = -\frac{1}{T}\left\{\left(\breve{g}_{\text{vb}} + g_\sigma \kappa\right)\frac{\mathrm{d}\eta}{\mathrm{d}t} + \Omega_\sigma\left[\frac{\partial}{\partial \ell}\left(\breve{g}_\sigma J_\sigma\right) + \breve{g}_\sigma(\hat{J}_{\text{b}} + \hat{J}_{\text{v}})\right]\right\}, \tag{33}$$

where the last term represents the REF, which can be immediately obtained from Eq. (5). $\hat{J}_{\text{v}}$ and $\hat{J}_{\text{b}}$ are the total atomic drift-diffusion fluxes at the reaction fronts separating the void and the interfacial layer and the

bulk and the interfacial layer, in orientations perpendicular to and normal to the interfacial layer, respectively.

The first group of terms in Eq. (33) represents the IEP density. The second group of terms represents, respectively, the divergence of the surface entropy flow (DEF) and the contribution due to lateral flow of entropy from exchange of chemical species between bulk phase and interface and/or void phase with the interface (evaporation and condensation). The interfacial layer including the void side is a completely open system (realistic void), and the displacement process is assumed isothermal. In order to calculate the global rate of entropy change along the whole curved interfacial layer, let us first take the line integral of Eq. (33) along the entire closed curved interface. Any possible singularity such as a triple junction that may be situated at a point denoted by the open interval $(-\varepsilon,\varepsilon)$ when $\varepsilon \to 0$ is excluded.

$$\int_{+\varepsilon}^{-\varepsilon} \mathrm{d}\ell \frac{\partial \hat{S}}{\partial t} = \lim_{\varepsilon\to 0} \oint_{\varepsilon} \mathrm{d}\ell \frac{\partial \hat{S}}{\partial t} = -\frac{1}{T} \lim_{\varepsilon\to 0} \left\{ \oint_{\varepsilon} \mathrm{d}\ell \left[\left(\breve{g}_{\mathrm{vb}} + g_\sigma \kappa \right) \frac{\mathrm{d}\vec{\eta}}{\mathrm{d}t} + \Omega_\sigma \left(\frac{\partial}{\partial \ell} \left(\breve{g}_\sigma J_\sigma \right) + \breve{g}_\sigma \hat{J}_{\mathrm{vb}} \right) \right] \right\}. \tag{34}$$

In the absence of particle sources or sinks, local normal interface motion is governed by a balance between the divergence of the atomic flux and the amount of mass accumulated or depleted at the interface. However, in this paper we consider the more general situation in which additional entropy source terms associated with the normal components of the atomic flow coming from the bulk phase $\hat{J}_{\mathrm{b}}$ and from the void region $\hat{J}_{\mathrm{v}}$ due to condensation or evaporation processes are included. These terms are additive $\hat{J}_{\mathrm{vb}} = \hat{J}_{\mathrm{v}} + \hat{J}_{\mathrm{b}}$. Hence the following rigorous expression applies for the conservation of atomic species during the virtual displacement of curved interphases having neither variation due to stretching nor in thickness:

$$[(c_{\mathrm{b}} - c_{\mathrm{v}}) - h_\sigma \bar{\kappa} c_\sigma] \frac{\mathrm{d}\eta}{\mathrm{d}t} = \sum_i \frac{\partial J_\sigma^i}{\partial \ell} - \sum_i (\hat{J}_{\mathrm{b}}^i + \hat{J}_{\mathrm{v}}^i) = \frac{\partial J_\sigma}{\partial \ell} - \hat{J}_{\mathrm{bv}}. \tag{35}$$

c_{b}, c_{v} and c_σ are the atomic volumetric concentrations associated with the bulk, void and surface phases, respectively. Assuming that a realistic void is a polyatomic dilute gas in which $c_{\mathrm{v}} = 0$ and $\bar{\kappa} h_\sigma = 0$, the following result is obtained:

$$\frac{\mathrm{d}\eta}{\mathrm{d}t} = \hat{n} \cdot \frac{\partial \vec{r}}{\partial t} = \Omega_{\mathrm{b}} \left(\frac{\partial J_\sigma}{\partial \ell} - \hat{J}_{\mathrm{vb}} \right), \tag{36}$$

where $\Omega_{\mathrm{b}} = c_{\mathrm{b}}^{-1}$ is adapted from the literature (Ogurtani and Oren, 2001; Guggenheim, 1959; Wang and Suo, 1996). $\vec{n}$ and $\vec{r}$ are the surface normal and the position vectors, respectively.

Substitution of Eq. (36) into the integrated entropy expression Eq. (34) gives:

$$\begin{aligned} \int_{+\varepsilon}^{-\varepsilon} \mathrm{d}\ell \frac{\partial \hat{S}}{\partial t} = -\frac{\Omega_\sigma}{T} \lim_{\varepsilon\to 0} \Bigg\{ & \int_{+\varepsilon}^{-\varepsilon} \mathrm{d}\ell \left[\left(\breve{g}_{\mathrm{vb}} + g_\sigma \kappa \right) \frac{\partial J_\sigma}{\partial \ell} \right] - \int_{+\varepsilon}^{-\varepsilon} \mathrm{d}\ell \left[\left(\breve{g}_{\mathrm{vb}} + g_\sigma \kappa \right) \hat{J}_{\mathrm{vb}} \right] \\ & + \int_{+\varepsilon}^{-\varepsilon} \mathrm{d}\ell \frac{\partial}{\partial \ell} \left(\breve{g}_\sigma J_\sigma \right) + \int_{+\varepsilon}^{-\varepsilon} \mathrm{d}\ell \left(\breve{g}_\sigma \hat{J}_{\mathrm{vb}} \right) \Bigg\}. \end{aligned} \tag{37}$$

The first and the third group of terms on the right hand side of the above relationship can be integrated by parts. Subsequently the rate of global entropy is split into the global IEP and the REF by carefully inspecting the individual contributions of each term (Ogurtani and Oren, 2001). The global IEP term is identified as:

$$\begin{aligned} \frac{\mathrm{d}}{\mathrm{d}t} S_{\mathrm{IEP}} = \frac{\Omega_\sigma}{T} \lim_{\varepsilon\to 0} \Bigg\{ & \int_{+\varepsilon}^{-\varepsilon} \mathrm{d}\ell \left[J_\sigma \frac{\partial}{\partial \ell} \left(\breve{g}_{\mathrm{vb}} + g_\sigma \kappa \right) \right] + \int_{+\varepsilon}^{-\varepsilon} \mathrm{d}\ell \left[\left(\breve{g}_{\mathrm{vb}} + g_\sigma \kappa \right) \hat{J}_{\mathrm{vb}} \right] - \left[\left(\breve{g}_{\mathrm{vb}} + g_\sigma \kappa \right) J_\sigma \right]_{-\varepsilon} \\ & + \left[\left(\breve{g}_{\mathrm{vb}} + g_\sigma \kappa \right) J_\sigma \right]_{+\varepsilon} \Bigg\}. \end{aligned} \tag{38}$$

Similarly, we can collect those terms in Eq. (38), which are clearly related to the rate of entropy flow, or in another words to the external entropy contribution associated with the void surface phase excluding the singular triple junction. Hence:

$$\frac{\mathrm{d}}{\mathrm{d}t}S_{\mathrm{REF}} = \frac{\Omega_\sigma}{T}\lim_{\varepsilon\to 0}\left\{-\int_{+\varepsilon}^{-\varepsilon}\mathrm{d}\ell\left(\breve{g}_\sigma \hat{J}_{\mathrm{vb}}\right) - \left[\breve{g}_\sigma J_\sigma\right]_{-\varepsilon} + \left[\breve{g}_\sigma J_\sigma\right]_{+\varepsilon}\right\}. \tag{39}$$

In these expressions $\breve{}$ denotes volumetric densities and $\hat{}$ denotes the bulk flux intensities ($\#\mathrm{m}^{-2}\,\mathrm{s}^{-1}$). Here, $J_\sigma = \sum_i J_\sigma^i$ denotes the sumover surface atomic drift-diffusion (convective) fluxes ($\#\mathrm{m}^{-1}\,\mathrm{s}^{-1}$) in the interfacial layer. Similarly, $\hat{J}_{\mathrm{b}} = \sum_i \hat{J}_{\mathrm{b}}^i$ and $\hat{J}_{\mathrm{v}} = \sum_i \hat{J}_{\mathrm{v}}^i$ are the total atomic drift-diffusion flux densities (convective) normal to the interface, and they are coming from the adjacent bulk and void phases, respectively. In this formulation, the total convective fluxes as well as the drift-diffusion fluxes associated with the individual chemical species are referred to the laboratory reference frame. Because, the whole interconnect material shows constant drift in the direction of the electron wind under the action of the externally applied electromigration forces having free boundary conditions at the cathode and the anode edges. Hence, neither the barycentric velocity complications of Prigogine (1961) entropy source term nor 'the simple isotropic elastic solid crystal' reference system (Haase, 1969) enters into the problem. However, in the total atomic drift-flux calculations, relevant summation operations do not include vacancies. Instead the rigorous identities $\hat{J}_{\mathrm{b}}^{\mathrm{V}} = -\hat{J}_{\mathrm{b}}$ and $J_\sigma^{\mathrm{V}} = -J_\sigma$ are valid. The superscript, $^{\mathrm{V}}$, denotes the vacancy drift-diffusion flux density in the relevant phase assuming that it has a crystalline structure. Without crystal structure such connection has no meaning.

In the absence of a singularity, the last two terms in Eqs. (38) and (39) vanish. It follows from the integrated internal entropy production, given by Eq. (38),

$$F_\sigma = \Omega_\sigma\left\{\frac{\partial}{\partial\ell}\left[\frac{1}{T}\left(\breve{g}_{\mathrm{vb}} + g_\sigma\kappa\right)\right] + \vec{t}\cdot\vec{F}_{\mathrm{Ext}}\right\} \tag{40}$$

and

$$F_{\mathrm{vb}} = \Omega_\sigma\left\{\left[\frac{1}{T}\left(\breve{g}_{\mathrm{vb}} + g_\sigma\kappa\right)\right] + \vec{n}\cdot\vec{F}_{\mathrm{Ext}}\right\}, \quad \text{(valid for ordinary points)}. \tag{41}$$

F_σ and F_{vb} denote longitudinal and transverse generalized forces that are acting on the interfacial layer respectively. In Eqs. (40) and (41) the fundamental connection between conjugated forces and fluxes have included an additional contribution due to the external forces $\vec{F}_{\mathrm{Ext}}$ as formulated in Appendix-B of Ogurtani and Oren (2001). $\vec{t}$ and $\vec{n}$ denote unit tangent and normal vectors at the void surface, respectively. The last contribution in Eq. (41) vanishes since the normal component of the electric field intensity and the traction vanish at the void surface. The conjugate fluxes associated with the above forces are identified by using the conventional approach of linear irreversible thermodynamics for isothermal processes in the presence of conservative external force fields. The surface flux is

$$J_\sigma = \frac{M_\sigma}{kT}\Omega_\sigma\frac{\partial}{\partial\ell}\left[\left(\breve{g}_{\mathrm{vb}} + g_\sigma\kappa\right) + \left|\langle eZ^*\rangle_\sigma\right|\frac{\vartheta}{\Omega_\sigma} + \left\langle\bar{\bar{\lambda}}\right\rangle_\sigma \otimes \bar{\bar{\sigma}}\right] \tag{42}$$

and the net lateral flux density responsible for the growth process is,

$$\breve{J}_{\mathrm{vb}} = \frac{M_{\mathrm{vb}}}{kT}\Omega_\sigma\left(\breve{g}_{\mathrm{vb}} + g_\sigma\kappa\right). \tag{43}$$

Cross coupling between generalized forces and fluxes has been neglected. M_σ/k and M_{vb}/k are generalized phenomenological mobilities associated with the respective conjugated forces and fluxes, and k is Boltzmann's constant. As described in Appendix-B of Ogurtani and Oren (2001), $\langle\bar{\bar{\lambda}}\rangle_\sigma$ is the mean value of the elastic dipole tensor associated with the atomic species, which are situated at the first nearest

neighboring sites of the vacancies in the interfacial layer. Here $tr\langle\bar{\bar{\lambda}}\rangle_\sigma \geqslant 0$ due to vacancy relaxation. $\langle eZ^*\rangle_\sigma \leqslant 0$ is the mean effective electromigration charge associated with the interacting chemical species in the surface layer. Double bars in the expressions indicate tensor quantities, and the $\otimes$operator denotes the enlarged double inner tensorial or dyadic product ($\bar{\bar{a}} \otimes \bar{\bar{b}} = a_{ij}b_{ij}$). For multi-component systems, we are interested only in the net atomic (mass) transport regardless of the contributions of individual chemical species. Thus, the first generalized-mobility given above may not be easily connected to any combination of intrinsic surface diffusivities of individual chemical species in the interfacial layer or in the bulk phase. However, for a one-component system having insignificant amounts of doping elements or impurities, a relationship between the generalized mobility and the surface self-diffusivity of host matter denoted by $\tilde{D}_\sigma$ is,

$$\hat{M}_\sigma = \frac{M_\sigma}{kT} = \frac{\tilde{D}_\sigma}{kT}\frac{h_\sigma}{\Omega_\sigma} = \frac{\tilde{D}_\sigma}{kT}\Gamma_\sigma. \tag{44}$$

In summary, the following compact form will be used,

$$J_\sigma = \hat{M}_\sigma \frac{\partial}{\partial \ell}\left[\Omega_\sigma\left(\breve{g}_{\mathrm{vb}} + g_\sigma\kappa\right) + \left|\langle eZ^*\rangle_\sigma\right|\vartheta + \Omega_\sigma\left\langle\bar{\bar{\lambda}}\right\rangle_\sigma \otimes \bar{\bar{\sigma}}\right]. \tag{45}$$

Eq. (45) takes additional driving forces such as the electromigration and the stress assisted drift motion of surface atoms into consideration. $\hat{M}_\sigma$ is defined as a surface atomic mobility, and has the dimensions of $(\mathrm{J}^{-1}\mathrm{s}^{-1})$. The generalized mobility $M_{\mathrm{vb}}\,(\mathrm{m}^2\,\mathrm{s}^{-1})$ associated with the incoming bulk diffusive flux is related to the rate of transformation of chemical species from bulk phase to the interfacial layer or vice versa, over an activation energy barrier denoted by ΔG^*_{vb}. Hence, the transition rate theory of chemical kinetics advocated by Eyring (Yeremin, 1979), can be applied so that $M_{\mathrm{vb}} = (\frac{kT}{h})\exp(-\frac{\Delta G^*_{\mathrm{vb}}}{kT})$, where h is Planck's constant. Here we will define a renormalized mobility $\hat{M}_{\mathrm{vb}} = M_{\mathrm{vb}}/kT\left(\mathrm{m}^2\mathrm{J}^{-1}\,\mathrm{s}^{-1}\right)$.

If one compares the first group of terms, in the generalized interfacial drift-diffusion flux formula denoted by Eq. (45) for one components systems, where specific Gibbs free energy density becomes equal to the chemical potential, with the relationship proposed by Rice and Chuang (1981), which is mostly employed in the literature (Zhang and Bower, 2001; Gungor and Maroudas, 2001; Liang and Suo, 2001), then one can see the sign conflict coming from the strain energy density contribution to the GFEDoT. The main reason for this discrepancy as stated in the introduction of this paper is the usage of the total Helmholtz free energy variance $\delta F = 0$, not the dissipation function, which is given by $\delta\wp = \delta(W - F) \geqslant 0$ in isothermal natural processes. The intuitive generalization of the dissipation function concept for the composite systems under thermal equilibrium into the power dissipation function $T\mathrm{d}S_{\mathrm{in}}/\mathrm{d}t \Leftarrow \mathrm{d}\wp/\mathrm{d}t \geqslant 0$ could result Gibbs free energies rather than Helmholtz free energies even in their formula, similar to the results of our rigorous micro-element theory. According to the above cited authors the surface flux density associated with the capillary and the strain energy forces for one components system is given by

$$J_\sigma = \frac{D_\sigma h_\sigma}{\Omega_\sigma kT}\nabla_\ell\left[\Omega_\sigma\left(-\frac{1}{2}\bar{\bar{\varepsilon}}_{\mathrm{b}} \otimes \bar{\bar{\sigma}}_{\mathrm{b}} + \gamma_\sigma\kappa\right)\right] \quad \text{(Rice and Chuang, 1981)}. \tag{46}$$

On the other hand, Eq. (45) takes the following form for a realistic void region, which can exchange species with the interfacial layer (open diathermal boundary) for one type of chemical species, without EM and elastic-dipole stress field interaction:

$$J_\sigma = \frac{D_\sigma h_\sigma}{\Omega_\sigma kT}\nabla_\ell\left[\Omega_\sigma\left(\left\{\breve{g}_{\mathrm{v}/\sigma} - \breve{g}_{\mathrm{b}/\sigma}\right\} + \gamma_\sigma\kappa\right)\right]. \tag{47}$$

As demonstrated in Appendix A in our previous paper (Ogurtani and Oren, 2001), by decomposing internal energy into thermal and elastic components, the specific Gibbs free energy density for solid can be written as:

$$\breve{g}_{\mathrm{b}} = \breve{u}_{\mathrm{b}}^{\mathrm{ther}} - T\breve{s}_{\mathrm{b}} - \frac{1}{2}\bar{\bar{\varepsilon}}_{\mathrm{b}} \otimes \bar{\bar{\sigma}}_{\mathrm{b}} \quad \text{and} \quad \breve{f}_{\mathrm{b}} = \breve{u}_{\mathrm{b}}^{\mathrm{ther}} + \frac{1}{2}\bar{\bar{\varepsilon}}_{\mathrm{b}} \otimes \bar{\bar{\sigma}}_{\mathrm{b}} - T\breve{s}_{\mathrm{b}}, \tag{48}$$

where $\breve{u}_{\mathrm{b}}^{\mathrm{ther}}$ denotes the thermal part of the internal energy density. Eq. (48) clearly shows that rigorous decomposition of the Gibbs (or Helmholtz) free energy into thermal and elastic parts is impossible since the entropy density $\breve{s}$ in general depends on the stress. In fact the Maxwell relationship in Gibbs representation $\{T, \bar{\bar{\sigma}}, x_i\}$ shows this dependence very clearly, such as:

$$\frac{\partial \breve{s}}{\partial \bar{\bar{\sigma}}}\Big|_{T,x_i} = \frac{\partial \bar{\bar{\varepsilon}}}{\partial T}\Big|_{\bar{\bar{\sigma}},x_i} = \frac{\bar{\bar{L}}\bar{\bar{\sigma}}}{T} \neq 0, \tag{49}$$

where $\bar{L}_{\bar{\bar{\sigma}}} = \bar{T}\frac{\partial \bar{\bar{\varepsilon}}}{\partial T}\big|_{\bar{\bar{\sigma}},x_i}$ is the latent heat tensor referred to the unstrained state, and it is related to the thermal strain tensor (Fung, 1965; Callen, 1960), which is deduced from the entropy density under a constant temperature and with five of the stress-components unchanged while keeping the composition invariant. However, as a first order approximation this splitting can be realized as follows: Taylor expansion of the entropy density with respect to the stress field at constant temperature and composition yields the following expression, by keeping only the first order term:

$$\breve{s}(T, \bar{\bar{\sigma}}, x_i) \cong \breve{s}_0^{\mathrm{ther}}(T, x_i) + \frac{\partial \breve{s}_0}{\partial \bar{\bar{\sigma}}}\Big|_{T,x_i} \otimes \bar{\bar{\sigma}} \Rightarrow \breve{s}_0^{\mathrm{ther}} + \frac{\bar{\bar{L}}^0_{\bar{\bar{\sigma}},T}}{T} \otimes \bar{\bar{\sigma}}, \tag{50}$$

where $\breve{s}_0^{\mathrm{ther}}(T, x_i)$ and $\bar{\bar{L}}^0_{\bar{\bar{\sigma}},T}$ are the entropy density and the latent heat in the unstrained state, respectively. Hence, one may decompose the Gibbs (or Helmholtz) free energy density into thermal and elastic parts,

$$\breve{g}_{\mathrm{b}} \cong (\breve{u}_{\mathrm{b}}^{\mathrm{ther}} - T\breve{s}_{\mathrm{b}}^{\mathrm{ther}}) - \frac{1}{2}\bar{\bar{\varepsilon}}_{\mathrm{b}} \otimes \bar{\bar{\sigma}}_{\mathrm{b}} - \bar{\bar{L}}^{\mathrm{b},0}_{\bar{\bar{\sigma}}} \oplus \bar{\bar{\sigma}}_{\mathrm{b}} = f_{\mathrm{b}}^{\mathrm{ther}} - \frac{1}{2}\bar{\bar{\varepsilon}}_{\mathrm{b}} \otimes \bar{\bar{\sigma}}_{\mathrm{b}} - \bar{\bar{L}}^{\mathrm{b},0}_{\bar{\bar{\sigma}}} \oplus \bar{\bar{\sigma}}_{\mathrm{b}} \tag{51}$$

and

$$\breve{f}_{\mathrm{b}} \cong (\breve{u}_{\mathrm{b}}^{\mathrm{ther}} - T\breve{s}_{\mathrm{b}}^{\mathrm{ther}}) + \frac{1}{2}\bar{\bar{\varepsilon}}_{\mathrm{b}} \otimes \bar{\bar{\sigma}}_{\mathrm{b}} + \bar{\bar{L}}^{\mathrm{b},0}_{\bar{\bar{\sigma}}} \oplus \bar{\bar{\sigma}}_{\mathrm{b}} = f_{\mathrm{b}}^{\mathrm{ther}} + \frac{1}{2}\bar{\bar{\varepsilon}}_{\mathrm{b}} \otimes \bar{\bar{\sigma}}_{\mathrm{b}} + \bar{\bar{L}}^{\mathrm{b},0}_{\bar{\bar{\sigma}}} \oplus \bar{\bar{\sigma}}_{\mathrm{b}}. \tag{52}$$

Hence, GFEDoT $\breve{g}_{\mathrm{vb}}$ between the two bulk phases namely, the matrix,'b' and the realistic void phase 'v' (the secondary phase particle), may be written by using the forward difference operator, Δ, as:

$$\breve{g}_{\mathrm{vb}} \cong \Delta_{\mathrm{bv}}\left\{\breve{f}^{\mathrm{ther}} - \frac{1}{2}(\bar{\bar{\varepsilon}} \otimes \bar{\bar{\sigma}}) - (\bar{\bar{L}}_{\underline{\sigma}} \oplus \bar{\bar{\sigma}})\right\}. \tag{53}$$

This is a general expression for the bulk Gibbs free energy of transformation for the flat interfaces associated with the solid-state phase transformations, and taking into account the stress field properly.

In the case of realistic voids containing chemical species in vapor state (gaseous phase), Eq. (53) takes the following form, which can be easily obtain from the standard chemical thermodynamic arguments, which are clearly presented in Guggenheim (1959):

$$\breve{g}_{\mathrm{vb}} \cong \left\{\breve{g}_{\mathrm{v}}(T, P_{\mathrm{v}}^{\dagger}) + \sum_i \frac{x_i^{\mathrm{v}}}{\Omega_{\mathrm{v}}} RTLn\left(\frac{P_{\mathrm{v},i}^{*}}{P_{\mathrm{v}}^{\dagger}}\right)\right\} - \left\{\breve{f}_{\mathrm{b}/\sigma}^{\mathrm{ther}} - \frac{1}{2}(\bar{\bar{\varepsilon}} \otimes \bar{\bar{\sigma}})_{\mathrm{b}/\sigma} - (\bar{\bar{L}}^{\mathrm{b},0}_{\bar{\bar{\sigma}},T} \oplus \bar{\bar{\sigma}}_{\mathrm{b}/\sigma})\right\}, \tag{54}$$

where $\breve{g}_{\mathrm{v}}(T, P_{\mathrm{v}}^{\dagger})$ is standard Gibbs free energy of the vapor phase, $P_{\mathrm{v},i}^{*}$ and x_i^{v} are partial fugacity and atomic fraction of the ith specie in the vapor, respectively. $P_{\mathrm{v}}^{\dagger}$ is an arbitrarily chosen standard pressure. Ω_{v} is the mean atomic volume in the gas phase adjacent to the interface. Due to the convection currents in the vapor region at moderate temperatures, and the basic assumption of thermal equilibrium in the system, it is clear that the gradients of Gibbs free energy of the vapor phase $\nabla \breve{g}_{\mathrm{v}} = 0$, as well as the temperature dependent part of the bulk Helmholtz free energy density $\nabla \breve{f}_{b/\sigma}^{\mathrm{ther}} = 0$ drop out completely. Therefore, only the stress

dependent parts of the specific Gibbs free energy density of the bulk phase evaluated adjacent to the interfacial layer (the reaction zone) prevails in the surface drift-diffusion flux equation:

$$J_\sigma = \frac{D_\sigma h_\sigma}{\Omega_\sigma kT}\nabla_\ell\left[\Omega_\sigma\left(\left\{\frac{1}{2}(\bar{\bar{\varepsilon}}\otimes\bar{\bar{\sigma}})_{\mathrm{b}/\sigma} + (\bar{\bar{L}}^{\mathrm{b},0}_{\bar{\bar{\sigma}}}\oplus\bar{\bar{\sigma}})_{\mathrm{b}/\sigma}\right\} + \gamma_\sigma\kappa\right)\right]. \tag{55}$$

The comparison of Eq. (46), obtained by Rice and Chuang (1981) and later by Suo and Wang (1994), and Eq. (55), which are rigorously obtained in this paper using the fundamental postulated of thermodynamics in connection with the sound mathematical manipulations, shows clearly the sign conflict in the strain energy contribution to the drift-diffusion flux. This conflict does not come from their improper attempt to split up the total Helmholtz free energy. It comes directly from their treatment of the natural processes including isothermal reversible changes, by following Herring's celebrated approach to this composite system, namely; they have all employed the total Helmholtz free energy variance $\delta\Sigma F = 0$ rather then the dissipation function variation $\delta\Sigma(W - F) \geqslant 0$, where equality is necessary condition for the reversible and inequality for the irreversible isothermal processes.

Actually, one can easily check the validity of our claim by analyzing a simple hypothetical system, namely; a solid grain (realistic void) embedded in a bulk matrix having exactly the same chemical composition, crystal structure and temperature with well defined interfacial layer as a boundary (i.e., large angle grain boundary). The whole system is loaded by hydrostatic stress system having uniform bulk modulus denoted by K. One can easily show that the strain energy density difference adjacent to the boundary layer is given by $(P^2_{\mathrm{v}/\sigma} - P^2_{\mathrm{b}/\sigma})/2K$, where $\bar{\bar{\sigma}} = -P\bar{\bar{I}}/3$. If one uses this expression in Eq. (53), GFEDoT becomes $\breve{g}_{\mathrm{vb}} \cong \breve{f}^{\mathrm{ther}}_{\mathrm{vb}} + (P^2_{\mathrm{b}/\sigma} - P^2_{\mathrm{v}/\sigma})/2K - tr\bar{\bar{L}}^{\mathrm{b},0}_{\bar{\bar{\sigma}}}(P_{\mathrm{b}/\sigma} - P_{\mathrm{v}/\sigma})$. According to the local formulation of IEP given by Eq. (16), one should have the following equality $\breve{g}_{\mathrm{vb}} + g_\sigma\kappa = 0$ for the complete physico-chemical equilibrium (the reversible isothermal process) at any ordinary point along the interface. One should also remember that $\breve{f}^{\mathrm{th}}_{\mathrm{vb}} = 0$; since the hypothetical solid grain (void), trapped in a bulk matrix has exactly the same composition and the same crystal structure, which may only have different orientations bounded by large angle grain boundaries, with the bulk matrix. Hence, one can obtained the following relationship for the ordinary points, which is the generalization of Laplace equation:

$$\left(\bar{P}^2_{\mathrm{v}/\sigma} - \bar{P}^2_{\mathrm{b}/\sigma}\right)/2K - tr\bar{\bar{L}}^{\mathrm{b},0}_{\bar{\bar{\sigma}}}\left(\bar{P}_{\mathrm{v}/\sigma} - \bar{P}_{\mathrm{b}/\sigma}\right) = g_\sigma\kappa \cong \left(\bar{P}_{\mathrm{v}/\sigma} - \bar{P}_{b/\sigma}\right)\bar{P}_\sigma/K. \tag{56}$$

The last relationship is written according to the recommendation by Callen (1960), who stressed that in most cases the latent heat tensor is very small, and it can be neglected. Here $\bar{p}_\sigma$ is the mean pressure and $\bar{P}_\sigma/K \Rightarrow -tr(\bar{\bar{\varepsilon}}_\sigma) > 0$ is dilatation of the interfacial layer, respectively. The last connection in Eq. (56) is a very interesting relationship, which is obtained by assuming that the entropy dependence on the stress is negligible. This expression is appeared first time in the literature, and shows a clear connection between the specific surface Gibbs free energy density and the interfacial tension $g_\sigma = \gamma\bar{P}_\sigma/K = -\gamma tr(\bar{\bar{\varepsilon}}_\sigma) > 0$. This formula also reveals the fact that interfacial tension is always positive $\gamma > 0$, even though whole system is under the hydrostatic pressure and it also shows that the interfacial layer, like in the present case $tr(\bar{\bar{\varepsilon}}_\sigma) < 0$, not necessarily should be subjected to tension, as pointed out by Bakker (1911) as cited by Defay et al. (1966), as a possibility without any proof. Finally, we have proven that the mean hydrostatic pressure of a realistic solid-state void in its own matrix is greater then the pressure of its surrounding bulk region adjacent to the interfacial layer, $\bar{P}_{\mathrm{v}/\sigma} \geqslant \bar{P}_{\mathrm{b}/\sigma}$, by using our irreversible thermodynamic theory of surfaces. On the other hand if one uses Eq. (46), the formula given by Rice and Chuang (1981), Suo and Wang (1994) and Gungor and Maroudas (2001) one gets completely opposite answers.

The positive sign of the strain energy density in Eq. (55) is extremely important for the surface drift-diffusion driven crack growth as well as the void morphological evaluations (fatal slit formation) under capillary, and EM forces in passivated thin film metallic interconnects. Close inspection of the flux equation

Eq. (55) immediately reveals that there is a flow of matter from low strain energy density region towards the high strain energy sites. Since at least in isotropic elastic solids, the strain energy density (hoop stress) and the curvature around the void surface layer have similar functional form (homomorphism). That means the direction of the mass flow due to strain energy gradient like capillary effect is always from low curvature regions towards the high curvature domains. That also means the strain energy density regardless of the nature of the stress whether it is compressive or triaxial tension will always act as a healing agent by filling up grooves at the expense of humps. Hence, the local stress risers and the surface roughness will disappear due time. This conclusion is strictly valid for the ordinary points at the surfaces and interfaces. The singular points such as grain boundary grooves, and internal voids trapped by grain boundaries should be analyzed carefully and independently. However, our recent extensive simulation work (Ogurtani and Akyildiz, 2004) on the grain boundary grooving and the cathode drifting shows that in the EM dominating regime $\chi \geqslant 1$ the groove depth has a finite asymptotic value, which is inversely proportional with the electron wind intensity parameter denoted by χ, which will be defined in the next section. The slowing down trend in the groove tip displacement is also observed by Averbuch et al. (2003b) in their recent but rather limited experiments, which are unfortunately too early terminated because of the extremely long computation time.

There is another important term in Eq. (45), which is directly related to the elastic-dipole interaction of point defects with the stress field such as mono-vacancies and interstitials. According to this term, there will always be a flow of matter via vacancies or interstitials, along the interfacial layers or at the surfaces, from the compression sites towards the tension regions, since in the case of isotropic point defects (mono-vacancies) the mean force per atom is given by $F_\sigma = 3^{-1}\Omega_\sigma \langle tr\bar{\bar{\lambda}}\rangle_\sigma \nabla_\ell (tr\bar{\bar{\sigma}})$. Therefore, for the hydrostatic triaxial tension loading (thermal contraction in passivated interconnects upon down cooling) there will be constant flow of matter to the grain boundary grooves at the surfaces (crack tips) or to the sharp corners of the interior voids acting as the stress risers. This matter flow generates healing effect by decreasing the curvatures of the sharp corners and relieving the local stress concentration similar to strain energy contribution to Gibbs free energy. Unfortunately, hydrostatic compressive stresses create just the opposite effects, they try to roughen the surfaces and deepen the grooves, and therefore they counter act the healing effects of the strain energy density, as mentioned above.

3. Mathematical model for the evolution dynamics of void intergranular motion

The present model, considers not only the drift-diffusion of chemical species along the realistic void surface, but also the direct transfer of chemical species between bulk phase and the void region through the interface layer (growth) as dominant transport mechanisms. Assuming no charged particles reside within the void region (perfect insulator) then the trans-granular and inter-granular motion of the void is determined from the velocities

$$\bar{v}_{\mathrm{ord}} = \frac{\partial}{\partial \bar{\ell}}\left[D''(\theta,\phi)\frac{\partial}{\partial \bar{\ell}}\left(\bar{g}_{\mathrm{vb}} + \chi\bar{\vartheta} + \bar{\kappa}\right)\right] - \overline{M}_{\mathrm{vb}}\left(\bar{g}_{\mathrm{vb}} + \bar{\kappa}\right) \tag{57}$$

and

$$\bar{v}_{\mathrm{g}}^{\mathrm{long}} = \overline{M}^{\mathrm{long}}\frac{\bar{\Omega}_{\mathrm{g}}\bar{d}_{\mathrm{a}}}{2\bar{\Omega}_\sigma^2\bar{h}_{\mathrm{g}}}\left[2\lambda - \left(\cos\theta^+ + \cos\theta^-\right)\right] \tag{58}$$

for ordinary points and triple junctions, respectively, and written in terms of normalized and scaled parameters and variables. The surface drift-diffusion has been assumed anisotropic which is included in the angular dependent post factor denoted by $D''(\theta,\phi)$.

The boundary conditions that apply at the triple junctions written in terms of right side $\bar{J}_0^-$ and left side $\bar{J}_0^+$ fluxes are

$$\bar{J}_0^+ = \bar{M}^{\text{long}} \frac{\bar{d}_a}{2\bar{\Omega}_\sigma^2}\left(\lambda - \cos\theta^+\right) + \frac{\bar{J}_g}{2} + \bar{J}_\vartheta - \bar{M}^{\text{trans}} \frac{\bar{d}_a}{\bar{\Omega}_\sigma^2}\left(\sin\theta^- - \sin\theta^+\right) \tag{59}$$

and

$$\bar{J}_0^- = -\bar{M}^{\text{long}} \frac{\bar{d}_a}{2\bar{\Omega}_\sigma^2}\left(\lambda - \cos\theta^-\right) - \frac{\bar{J}_g}{2} + \bar{J}_\vartheta - \bar{M}^{\text{trans}} \frac{\bar{d}_a}{\bar{\Omega}_\sigma^2}\left(\sin\theta^- - \sin\theta^+\right). \tag{60}$$

$\bar{J}_g$ and $\bar{J}_\vartheta$ denote the normalized atomic fluxes associated with grain boundary flow, and the drift-diffusion at the junction due to electromigration, respectively. The grain boundary flux due to of electromigration is given by $\bar{J}_g = -\bar{M}_{gb}[\chi(\hat{n}_g \cdot grad\bar{\vartheta})/\bar{\Omega}_g]$. In the above relationships, the explicit expressions for the mobilities are given by

$$\hat{M}^{\text{long}} = \frac{\Re^{\text{long}}}{kT}\frac{h_g}{\Omega_g}, \quad \hat{M}^{\text{trans}} = \frac{\Re^{\text{trans}}}{kT}\frac{h_\sigma}{\Omega_\sigma} \quad \text{and} \quad \hat{M}_\sigma = \frac{D_\sigma^0}{kT}\frac{h_\sigma}{\Omega_\sigma}, \tag{61}$$

$\bar{M}^{\text{long}}$ is the ratio of the longitudinal mobility of the triple junction to the surface mobility $\hat{M}_\sigma$.

In above formulas the bar sign over letters indicates the following scaled and normalized quantities, which are given by

$$\bar{w} = w/r_0, \quad \bar{t} = t/\tau_0, \quad \bar{\ell} = \ell/r_0, \quad \bar{\kappa} = \kappa r_0, \tag{62}$$

$$\bar{g}_{vb} = \frac{\breve{g}_{vb} r_0}{g_\sigma}, \quad \bar{\vartheta} = \vartheta/(E_0 r_0), \quad \text{and} \quad \chi = e\left|\breve{Z}\right| E_0 r_0^2/(\Omega_\sigma g_\sigma). \tag{63}$$

Similarly the generalized mobility $\hat{M}_{vb}$ associated with interfacial displacement reaction taking place during the void growth process has been normalized so that $\bar{M}_{vb} = \hat{M}_{vb} r_0^2/\hat{M}_\sigma$.

In the above description the time scale $\tau_0 = r_0^4/(\Omega_\sigma^2 \hat{M}_\sigma g_\sigma)$, and the length scale r_0 is the initial mean radius of the void, which can be obtained from the cross sectional area. w is the interconnect half-width, E_{el} is the proper elastic modulus, Ω_σ is the atomic volume in the void surface layer, $\tilde{D}_\sigma \delta_\sigma$ is the thickness of the surface layer times its diffusivity, k is the Boltzmann's constant, T is the absolute temperature and ϑ is the electrostatic potential generated at the void surface due to the remote applied electric field denoted by E_0.

The first group of terms in the above partial differential equation (Eq. (57)) represents mass accumulation due to surface diffusion along the void interfacial layer. The second group of terms, which appears for the first time in the literature in Ogurtani and Oren (2001), is due to the mass flow associated with the chemical species transfer (vacancy flow in opposite direction) between bulk phase and a void region having a curved advancing reaction front.

The numerical methods employed in the present studies are summarized in our previous paper (Ogurtani and Oren, 2001), and will not be repeated here. The anisotropic diffusivity of surface atoms is modeled by defining

$$\widetilde{D}_\sigma(\theta, \phi) = D_\sigma^0\left\{1 + A\cos^2[m(\theta + \phi)]\right\}, \tag{64}$$

where D_σ^0 is the minimum surface diffusivity corresponding to a specific surface orientation, θ is the angle formed by the local tangent to the surface and the direction of the applied electric field. A, m, and ϕ are dimensionless parameters that reflect the strength of the anisotropy, the group symmetry of the crystal giving rise to "easy" diffusion orientations, and the orientation of the crystal with respect to the direction of the applied electric field E_0, respectively. For brevity the angular dependent part of the diffusivity in above equations is denoted by $D''(\vartheta, \theta)$ and $N = 2m$ corresponds to the degree of rotational symmetry.

4. Results and discussions

In order to test the efficiency of the numerical methods, and the validity of the irreversible thermodynamic theory proposed by Ogurtani (2000), a series of computer simulation experiments are performed assuming that the specific Gibbs free energies associated with the void surface layer and the grain boundary are completely isotropic. In these simulations, only those interconnect ribbons having a bamboo structure with equally spaced grain boundaries perpendicular to the applied electric field are considered. In order to facilitate data interpretation, void growth and mass flow from the grain boundary to the triple junction are neglected.

In Fig. 2, snapshots of the void grain boundary interaction are presented using two different wetting parameters, namely $\lambda = 0.8$ and $\lambda = 1$ (complete wetting). Only capillary forces are taken into account.

Fig. 2 shows that the void–grain boundary system starts to evolve towards the equilibrium configuration as soon as the grain boundary and void come into close contact with each other. The equilibrium configuration has dihedral angles dictated by thermostatic theory, i.e. $\theta_{eq}^{+} = \arccos\left(\lambda^{+}\right)$ and $\theta_{eq}^{-} = \arccos\left(\lambda^{-}\right)$ for the left and right sides respectively. The rate of shape evolution seems to be controlled by the surface drift-diffusion mobility, the generalized mobilities associated with longitudinal movement of the triple junction and the transverse flow of matter through the junction.

In Fig. 3, void intergranular motion and shape evolution under the action of capillary and electromigration forces are presented in a series of snapshots. The normalized interconnect half line width is $\bar{w} = 1$, the wetting parameter $\lambda = 0.8$ and the normalized electron wind intensity is selected to be $\chi = 100$. Fig. 3 shows the void penetration through, and then detachment from the grain boundary, with simultaneous formation of a daughter void at the advancing front. Similar phenomena have been observed by Schimschak and Krug (2000). The effect of capillary forces is more clearly illustrated as the sharp (slit-like) tail of the void

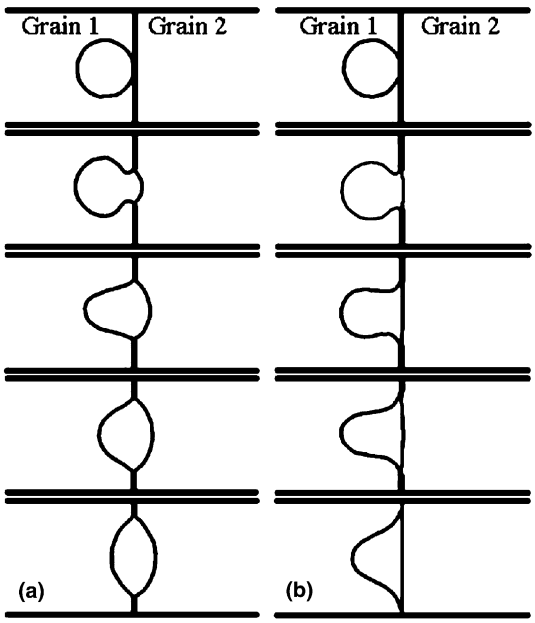

Fig. 2. Snapshots showing the dynamical evolution of the void-grain boundary system towards the equilibrium configuration under the action of capillary without electromigration forces ($\chi = 0$). Interfacial diffusion is isotropic and there is no void growth. (a) $\lambda = 0.8$, (b) $\lambda = 1$ (complete wetting).

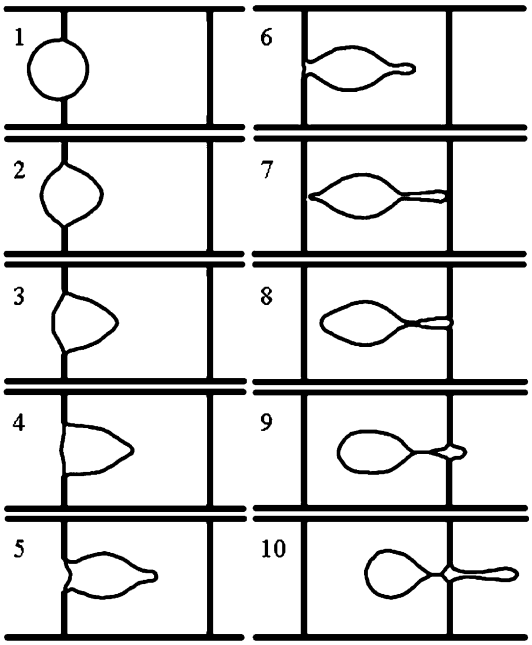

Fig. 3. Snapshots showing grain-boundary detachment and fragmentation of a void during intergranular motion under the action of capillary and electromigration stresses. The interfacial diffusion is isotropic and there is no void growth. The electron wind intensity, $\chi = 100$, the wetting parameter, $\lambda = 0.8$ and the scaled line width $\bar{w} = 2.0$.

starts to round up just after the detachment (detrapping) stage is completed. In the final phase of the simulation, the daughter void penetrates into the neighboring grain boundary, while the parent void is left behind. The triple junction behavior is highly dynamical, showing large and time dependent departure from the equilibrium configuration, which is contrary to the constraints enforced in many theoretical treatments presented in the literature (Chuang and Rice, 1973; Pharr and Nix, 1979; Huang et al., 2000; Needleman and Rice, 1980; Pan and Cocks, 1994, 1995; Cocks, 1994; Kucherenko et al., 2000; Khenner et al., 2001; Ohring, 1971; Takahashi et al., 1991; Gottstein and Shvindlerman, 2002; Mullins, 2001; Liu et al., 2001; Mahadevan and Bradley, 1999; Cahn and Hilliard, 1958).

The importance of texture on electromigration failure associated with a void trapped at a high energy grain boundary in a bamboo type interconnect is illustrated by simulating of 36 distinguishable (eliminating mirror symmetry elements) variations in adjacent grain textures by incorporating anisotropic surface diffusivities. (Typical morphologies are presented here as snapshots. However the full template of results from this study and the evaluation of results in terms of effective failure times and pattern formation will be published in a separate paper.) In Fig. 4, the evolution of a void that is initially cylindrical in shape and trapped by a high energy grain boundary separating two bamboo grains both having (1 1 0)–[1 1 0] texture is simulated for different misorientation angles. In these simulations, the normalized interconnect half width $\bar{w} = 2.5$, the electron wind intensity $\chi = 10$, the wetting parameter $\lambda = 0.8$ and the interface controlled reaction and the rate of condensation of the athermal vacancies in this supersaturated bulk material are given by $\Delta\bar{g}_{vb} = -5$ and $\bar{M}_{vb} = 5$, respectively.

In Fig. 4a, in which both grains lie along the direction of the applied electric field, evolution of a void without detrapping is completely symmetric. Eventually edge cuts occur at both sides of the interconnect by the formation of a double slit. The premature failure has a normalized effective failure (NEF) time of approximately $\bar{t}_F = 0.248$.

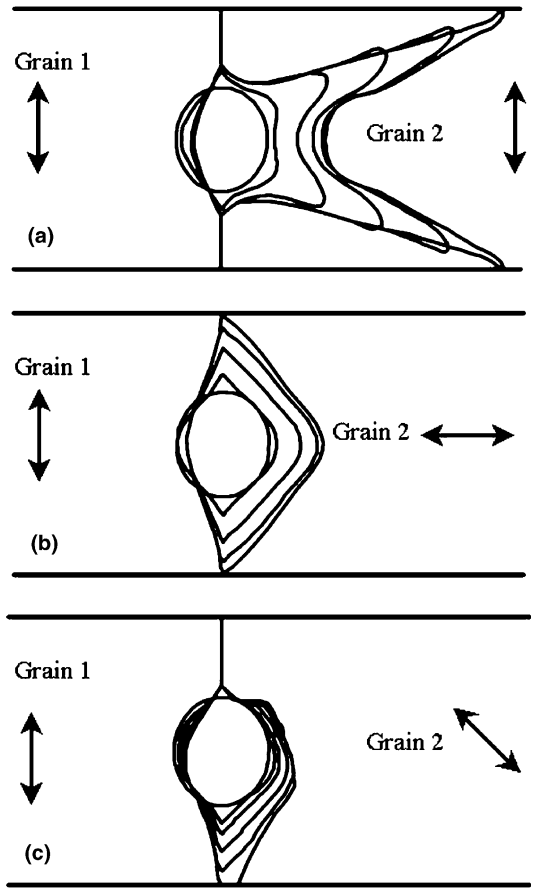

Fig. 4. Morphological evolution of a circular void nucleated initially on a grain-boundary interconnect with bamboo structure having well defined grain-textures. Interfacial diffusion is anisotropic and the void grows ($\Delta\bar{g}_{vb} = -5,\ \bar{M}_{vb} = 5$). The electron wind intensity $\chi = 10$, the wetting parameter, $\lambda = 0.8$ and the scaled line width $\bar{w} = 2.5$. Grain 1: $m = 1$, $A = 5$, $\theta = 0$. (a) Grain 2: $m = 1$, $A = 5$, $\theta = 0$, $\bar{t}_F = 0.248$. (b) Grain 2: $m = 1$, $A = 5$, $\theta = 90$, $\bar{t}_F = 0.146$. (c) Grain 2: $m = 1$, $A = 5$, $\theta = 45$, $\bar{t}_F = 0.074$.

In Fig. 4b, the results of a computer simulation on a sample having nearly the same system parameters as the previous example except that the (110)–[110] texture on the wind-side of the grain boundary is tilted by 90° in an anticlockwise direction with respect to the incoming electron wind. Under these conditions the results show that the failure mechanism is a two-sided grain boundary tearing mode having shorter NEF—time for the premature interconnect failure, $\bar{t}_F = 0.146$. This is completely different than in the results presented in Fig. 4a.

In Fig. 4c, the texture on the left side is the same as in the two previous cases, but the wind-side is rotated 45° in an anti-clock wise direction with respect to the incoming electron wind. In this simulation, the void evolves asymmetrically towards the lower edge of the grain boundary. Failure of the interconnect occurs by the one-sided grain boundary tearing failure mechanism. This premature failure has an elapsed NEF—time $\bar{t}_F = 0.074$.

It has been shown that among all possible modes associated with the grain boundary cavity evolution dynamics the one-sided grain boundary tearing mode (upper or lower edges) is the most detrimental electromigration failure mechanism for metallic interconnects having bamboo structure.

In order to evaluate the effect of current crowding on the morphology as well as on the mean time to failure MTTF of the interconnect, additional sequences of void grain boundary interaction simulation experiments are performed. The wetting parameter $\lambda_{Al} = 0.165$, which is valid for aluminum interconnects (Liu et al., 2001). The profound effect of the normalized electron wind intensities χ on the shape evolution dynamics is observed in narrow interconnects when the size of the void is comparable to the line width ($\bar{w} \leqslant 2.5$).

This unique behavior is presented in Fig. 5, by the sequence of snapshots that are taken just at the onset of the void detachment or detrapping process. Three different normalized interconnect widths are considered, namely $\bar{w} = 1.5$, $\bar{w} = 2.0$ and $\bar{w} = 2.5$.

In Fig. 6, the results of computer simulation experiments for different normalized line widths under a wide range of normalized electron wind intensities are presented in a plot of the normalized void detachment time, $\bar{t}_d$, as a function of χ and $\bar{w}$.

The plot reveals that all experimental points for a fixed normalized line width lie on a straight line. The analytical representation of the normalized void detachment time as a function of the electron wind intensity is determined to be: $\bar{t}_d(\bar{w}, \chi) = \alpha(\bar{w})\chi^{s(\bar{w})}$. In this expression, the slopes and the intercepts associated with the individual void detachment experiments are represented by $s(\bar{w}) = -1.155(1 - (\bar{w} + 0.5)^{-5})$ and $\alpha(\bar{w}) = 1.35(1 - \bar{w}^{-2.7})$, respectively. In general beyond the current crowding region $\alpha(\bar{w})$ may be assumed to have the value 1.35 because the analytical expression shows complete independence of $\alpha(\bar{w})$ on the line width as long as it is in range of $\bar{w} \geq 2.5$. For $\bar{w} \geqslant 2.5$ current crowding is completely negligible. According to our preliminary studies this prefactor may be slightly affected by the wetting parameter λ. Similarly, the

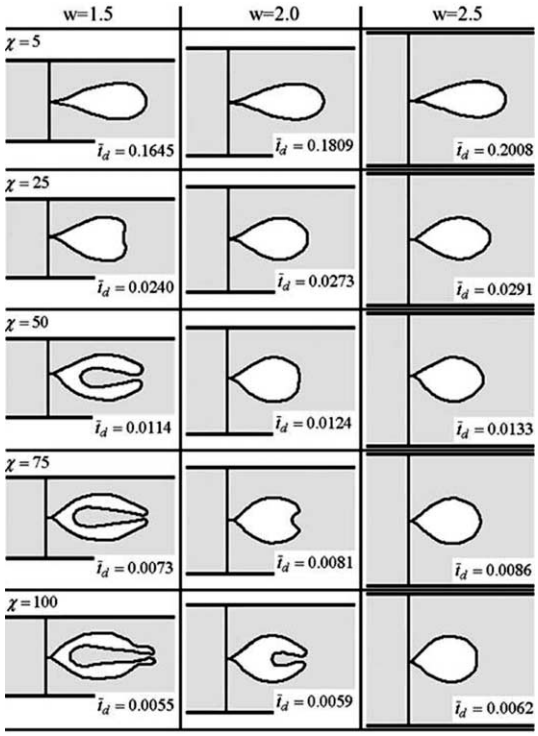

Fig. 5. A sequence of snapshots taken just at the onset of the void detachment process for several normalized electron wind intensities under various normalized line widths. The wetting parameter $\lambda = 0.165$.

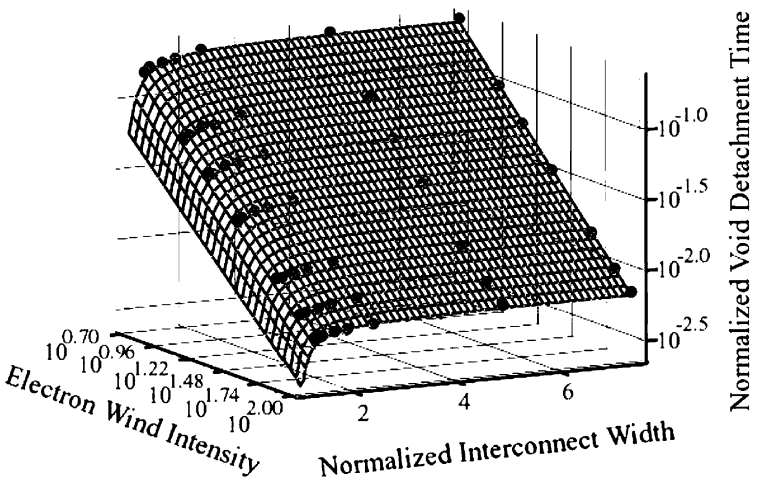

Fig. 6. The plot of void normalized detachment time vs. electron wind intensity and normalized interconnect width for bamboo lines.

slope or the quasi-current exponent $s(\bar{w})$ shows an almost complete independence from the line width in the range $\bar{w} \geqslant 2.5$, where $s(\bar{w})$ asymptotes to the value -1.155.

In terms of dimensional variables, the analytical results deduced from Fig. 6, give the void–grain boundary detachment time:

$$t_{\mathrm{d}} = \alpha(w, r_0) \frac{kTr_0^{4+2s(w,r_0)}}{D_\sigma h_\sigma (g_\sigma \Omega_\sigma)^{1+s(w,r_0)}} (eZ\rho j)^{s(w,r_0)}(s). \tag{65}$$

Eq. (65) indicates that the apparent activation enthalpy H_{App} of the detachment reaction is

$$H_{\mathrm{App}} = \frac{\mathrm{d}\ln(t_{\mathrm{d}})}{\mathrm{d}\left(\frac{1}{kT}\right)} \cong H_\sigma^{1V} - kT + \frac{\mathrm{d}\ln\alpha}{\mathrm{d}\left(\frac{1}{kT}\right)} = H_\sigma^{1V} - kT + \frac{\partial\ln\alpha}{\partial\ln\bar{M}} \frac{\mathrm{d}\ln\bar{M}}{\mathrm{d}\left(\frac{1}{kT}\right)} + \frac{\partial\ln\alpha}{\partial\ln\lambda} \frac{\mathrm{d}\ln\lambda}{\mathrm{d}\left(\frac{1}{kT}\right)}, \tag{66}$$

where by definition $H_\sigma^{1V} = -\mathrm{d}\ln(D_\sigma)/\mathrm{d}(1/kT)$ corresponds to the activation enthalpy of the void surface diffusivity, $H_\sigma^{1V} = H_\sigma^{1V,\mathrm{M}} + H_\sigma^{1V,\mathrm{F}}$ for the case in which thermal vacancy concentration is much greater than athermal (excess) vacancy concentration in the sample, otherwise $H_\sigma^{1V} = H_\sigma^{1V,\mathrm{M}}$.

Eq. (66) indicates that H_{App} may or may not be predominately determined by the activation enthalpy $H_\sigma^{1V,\mathrm{M}}$ of mono-vacancy motion along the void surface layer. This is true not only because of the contributions to H_{App} from the formation enthalpy of thermal vacancies $H_\sigma^{1V,\mathrm{F}}$, and from the $-kT$ term (≈ -0.025 eV at room temperature) but also because of the connection between the prefactor $\alpha(\bar{w})$ and the generalized mobilities.

Schreiber (1981) predicted that the enthalpy of vacancy motion at oxide-free surfaces of aluminum is equal to 0.28 eV. He also suggested that this value might be taken as the activation enthalpy of void surface diffusion by further assuming that the energy of vacancy formation is zero at the surface layers due to the presence of excess vacancies. This enthalpy should be observed only at the oxide-free surfaces, for instance at voids or holes inside the aluminum. According to Wang and Suo (1996) for those voids formed at the technical surfaces this value should be replaced by 0.71 eV. But our findings, which rely on the evaluation of published experimental data, indicate that the diffusion activation enthalpy for aluminum and aluminum alloys takes two distinct values, namely 0.62 eV if the nucleation site is at the interior of the unoxidized grain boundary or 0.84 eV if the nucleation site is at the triple junction between the technical surface and the oxidized grain boundary.

The third and especially the fourth terms of Eq. (66) contribute an additional component to the apparent or effective activation enthalpy of the detachment process. These arise from the temperature dependence of the generalized mobilities identified from the expression for the longitudinal and transverse triple junction displacements. In order to obtain a quantitative measure of this contribution, additional systematic and extensive simulation studies are required that span a wide range of values for the generalized mobilities $\bar{M}^{\text{long}}$ and $\bar{M}^{\text{trans}}$. From these simulations a correlation between the $\alpha(\bar{w})$ prefactor and the generalized mobilities is determined.

Deeper insight is gleaned by combining our findings with the analytical theory of Ho (1970), which gives the steady-state velocity of a circular void in an infinite conductor as $v = 2\Omega_\sigma \hat{M}_\sigma e\hat{Z}\rho j/r_0$. Therefore, the mean flight time for a void between two successive bamboo grain boundaries may be estimated as $t_{\text{flight}} = \ell_g/v = \ell_g r_0/(2\Omega_\sigma \hat{M}_\sigma e\hat{Z}\rho j)$, where ℓ_g is the mean distance between bamboo grain boundaries (grain size). Since detachment and flight constitute two series or consecutive unit operations leading to failure, the effective cathode-pad failure time (CPFT) associated with a void initially nucleated at the n_b^{th} bamboo grain is:

$$t_F(n_b) = \frac{n_b}{3600}\left[\alpha(w,r_0)\frac{kTr_0^{4+2s(w,r_0)}}{D_\sigma h_\sigma (g_\sigma \Omega_\sigma)^{1+s(w,r_0)}}(eZ\rho j)^{s(w,r_0)} + \frac{(\ell_g - 2r_0)r_0 kT}{2D_\sigma h_\sigma}(eZ\rho j)^{-1}\right](h). \tag{67}$$

In Eq. (67) n_b is the mean number of bamboo grain boundaries that a void crosses before it contributes to the full breach of the cathode pad. In the above expression the constraint imposed on the normalized line width is $w \geqslant r_0$ and on the grain size is $\ell_g \geqslant 2r_0$. These constraints eliminate any possible overlap between two successive detachment events that a given void may undergo before reaching the cathode pad or stud. Moreover, this formula does fully take into account the effect of current crowding. In our formulation of the CPFT, it is assumed that interconnect failure takes place by the migration and accumulation of voids, which have been trapped or nucleated at grain boundaries located at the cathode end of the line. Migration of voids is due to the action of applied electromigration forces. According to Basaran et al. (2003) as soon as a single void reaches the cathode pad this would create measurable degradation at the solder joint (e.g. a 5% drop in electrical resistance in the US micro-electronic industry). A brief representation of such a failure mechanism is illustrated in Fig. 7.

The upper bound of the cathode failure time (UBCFT) can be estimated by assuming that the grain boundary in the neighborhood of the anode may also contribute to the CPFT phenomenon by dismissing only one void. This void has the largest size $r_0 \cong r_{\max}$ allowable that can still break down the electrical

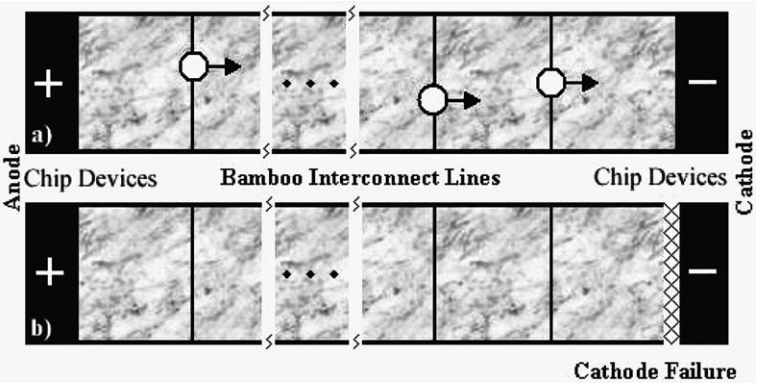

Fig. 7. Cathode pad failure mechanism by loosing the electrical contact at the cathode. (a) Interconnect with initially nucleated voids (b) failed interconnect.

contact at the cathode pad by means of current crowding effects. The upper value of $n_b = (L/\ell_g) - 1$ where L is the interconnect length. n_b is estimated by knowing the location of the grain boundary adjacent to the anode pad. Substitution of n_b in to Eq. (67) gives an expression for the UBCFT:

$$\mathrm{UBCFT} = \frac{\frac{L}{\ell_g} - 1}{3600}\left[\alpha(w, r_{\max})\frac{kTr_{\max}^{4+2s(w,r_{\max})}}{D_\sigma h_\sigma (g_\sigma \Omega_\sigma)^{1+s(w,r_{\max})}}(eZ\rho j)^{s(w,r_{\max})} + \frac{(\ell_g - 2r_{\max})r_{\max}kT}{2D_\sigma h_\sigma}(eZ\rho j)^{-1}\right](h). \tag{68}$$

The lower bond cathode failure time (LBCFT) can also be estimated using the following argument. Eq. (67) indicates that an interior void that is nucleated or trapped at a grain boundary and which has a radius precisely at the threshold level for detrapping is more likely to contributing to catastrophic failure of interconnects at the cathode pads than any other larger interior void. Consequently the LBCFT for interconnects with bamboo or even near-bamboo structures may be calculated by considering only those voids having threshold or critical size for detrapping. In order to find the threshold value the necessary simulation experiments and the analysis of the relevant data were carried out. Results gave the following expression for the threshold value of the applied normalized electron wind intensity for given normalized line width:

$$\chi(\bar{w}) = 1.53\left(1 - \frac{1.3}{\bar{w}^2}\right). \tag{69}$$

Written in terms of dimensional quantities:

$$r_{\mathrm{crt}}(w, j) = \left(\frac{1.3}{w^2} + \frac{eZ\rho j}{1.53 g_\sigma \Omega_\sigma}\right)^{-1/2}. \tag{70}$$

This expression indicates that the asymptotic value of the critical radius, which corresponds to zero current density, is $r_{\max} = w/\sqrt{1.3}$. The physical meaning of this asymptotic void radius is that it represents an upper bound in size of void that can permanently attach to a grain boundary under an applied electric field, regardless of intensity, because of the localized enhancement in the wind tearing force due to current crowding. In the case of moderate to high current density (for aluminum having a line width in the range of one micron $j \geqslant 10^9$ A/cm^2) the critical radius takes the form $r_{\mathrm{crt}}(j) = \sqrt{1.53 g_\sigma \Omega_\sigma / eZ\rho j}$, which is independent of the interconnect width. Therefore the LBCFT of an interconnect with bamboo or near-bamboo structures may be calculated by considering only those voids having threshold or critical size for detrapping, which is given by Eq. (70). Substitution of Eq. (70) into Eq. (67) for the value of r_0, and taking $n_b = 1$, the following expression for the LBCFT is found.

$$\mathrm{LBCFT} = \frac{1}{3600}\left\{\alpha(w, r_{\mathrm{crt}}(w,j))\frac{kT(r_{\mathrm{crt}}(w,j))^{4+2s(w,r_{\mathrm{crt}}(w,j))}}{D_\sigma h_\sigma (g_\sigma \Omega_\sigma)^{1+s(w,r_{\mathrm{crt}}(w,j))}}(eZ\rho j)^{s(w,r_{\mathrm{crt}}(w,j))} + \frac{(\ell_g - 2r_{\mathrm{crt}}(w,j))\cdot r_{\mathrm{crt}}(w,j)kT}{2D_\sigma h_\sigma}(eZ\rho j)^{-1}\right\}(h) \tag{71}$$

with the constraint: $\ell_g \geqslant 2r_{\mathrm{crt}}(w, j)$.

Since only values of the median time to failure (MTTF) or the time for 50% failure are reported in the literature, a naive statistical approach may be applied to Eq. (67). Assume that each grain boundary is a potential site for the nucleation and growth of a void having critical size and that test specimens are equally partitioned by the bamboo grains. Then only those grain boundaries which are situated at the mid positions of the sampling interconnects and ejecting voids with critical size will contribute to the measured values of MTTF. Hence, the following expression for the MTTF can be deduced from Eq. (67):

$$\mathrm{MTTF} = \frac{L}{3600\ell_g}\left\{\alpha(w, r_{crt}(w,j))\frac{kT(r_{crt}(w,j))^{4+2s(w,r_{crt}(w,j))}}{D_\sigma h_\sigma (g_\sigma \Omega_\sigma)^{1+s(w,r_{crt}(w,j))}}(eZ\rho j)^{s(w,r_{crt}(w,j))} + \frac{(\ell_g - 2r_{crt}(w,j))\cdot r_{crt}(w,j)kT}{2D_\sigma h_\sigma}(eZ\rho j)^{-1}\right\}(h). \tag{72}$$

In order to avoid overlap, the constraint $\ell g \geqslant 2r_{crt}(w,j)$ is required. This expression provides a concise form valid outside the current crowding regime that corresponds to the moderate and high current density domains:

$$\mathrm{MTTF}^0 = \frac{1.35L}{3600D_\sigma h_\sigma}\left[\frac{1.53kT\Omega_\sigma g_\sigma}{\ell_g}(Ze\rho j)^{-2} + \frac{(\ell_g - 2r_{crt}(j))\sqrt{1.53kT\Omega_\sigma g_\sigma}}{2\ell_g}(Ze\rho j)^{-3/2}\right](h)(\bar{w} \geqslant 2.5). \tag{73}$$

A close inspection of Eqs. (72) and (73) shows that limiting value of the current exponent outside the current crowding region varies from -1.5 to -2 depending upon the applied current density and the grain size. Specimens having small grain size and that are exposed to large current densities are dominated by the void detachment process, which results in a current exponent $n = -2$. On the other hand at moderate and large grain sizes failure is controlled by the void flight time and the resulting current exponent becomes $n = -1.5$. In the case of the current crowding regime, which appears at low current densities independent of grain size, the exact formula for the MTTF shows very different behavior, namely $n = -1$. This value cannot be predicted by the MTTF^0 formula because of the limitations discussed above.

In order to test the prediction power of these results, they are compared to the experimental findings in the literature in terms of the MTTF and the temperature or current density. In Fig. 8 the experimental MTTF versus inverse temperature data, reported by three different authors (Lytle and Oates, 1992; Black, 1969; Schreiber and Grabe, 1981) for aluminum interconnects with bamboo and polycrystalline materials having fine and large grain microstructures, are presented on a semi-logarithmic plot. Superimposed on the plot are the best matching LBCFT curves with and without flight time contributions. The experimental findings by Lytle and Oates (1992) for the no-void bamboo specimens and by Black (1969) for large grain polycrystallites are analyzed by LBCFT curve fittings with and without flight time contributions. This results in new diffusion coefficients for the void $D = 6.0 \times 10^{-6}\exp(-0.\ 84\ \mathrm{eV}/kT)\ \mathrm{m}^2\ \mathrm{s}^{-1}$ and/or for the technical surface atomic migration $D = 7.0 \times 10^{-6}\exp(-0.\ 84\ \mathrm{eV}/kT)\ \mathrm{m}^2\ \mathrm{s}^{-1}$. Test specimens used by these

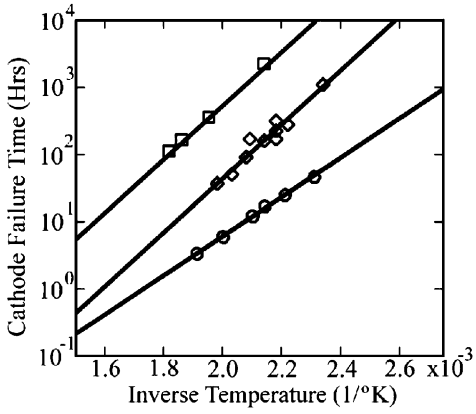

Fig. 8. Theoretical cathode failure time vs. inverse temperature on a semi-logarithmic plot; ◇: Near bamboo lines, Lytle and Oates (1992); CFT scaled-up with a factor of 10. □: Bamboo lines, Black (1969); CFT scaled-up with a factor of 100. ○: Polycrystalline lines, Schreiber and Grabe (1981).

authors have median line width versus grain size ratios of about $2w/l_g = 1.0$ (near-bamboo) and $2w/l_g = 1.9$ (large poly-grains), respectively, which are also tested at different current densities. The HVSEM shows that the void responsible for the line failure is nucleated at the Al/SiO_2 interface, and most probably at the triple junction between the intersecting grain boundary and the technical surface. This also explains why the activation enthalpies for these specimens are so high. Because of the contamination of the void surface by oxygen and silicon atomic species during the nucleation stage, a new set of trap centers for the vacancies are created, which inhibits their motion by contributing an extra binding energy E_B to the activation enthalpy of motion H_M. In addition contamination may cause substantial decrease in concentration as well. The existence of the effect of contamination is strongly supported by high-resolution SEM experiments recently reported by Marieb et al. (1995).

The most interesting feature in Fig. 8 is in the analysis of the data for a fine grain polycrystalline aluminum as presented by Schreiber and Grabe (1981) in terms of LBCFT formula without the flight time contribution ($\ell_g \cong r_{crt}$). The microstructural information provided by these authors indicates that the line width versus grain size ratio is about equal to 32. For the polycrystalline case, the LBCFT theory developed in this paper for bamboo structures results in a best fit by employing a diffusion coefficient for void surface mass transfer of $D_\sigma = 1.10 \times 10^{-6}\exp(-0.62\ \text{eV}/kT)\ \text{m}^2\ \text{s}^{-1}$.

In Fig. 9 the upper and lower bound cathode failure times together with the theoretical MTTF curves are plotted as a function of applied current density for the three different sets of aluminum interconnects with bamboo or near-bamboo structure. The log–log plot is constructed using Eqs. (68), (71) and (72). The aluminum interconnect test materials chosen use structural parameters deduced from a number of experimental studies. Data is taken from (1) Longworth and Thompson (1992) in bicrystal aluminum lines: $2w_0 = 2.0\ \mu\text{m}$, $L = 1000\ \mu\text{m}$, $\ell_g = 500\ \mu\text{m}$, $j = 2.5\ \text{MA cm}^{-2}$ and $T = 523\ \text{K}$, (2) Kinsbron (1980): $2w_0 = 1.0\ \mu\text{m}$, $L = 250\ \mu\text{m}$, $\ell_g = 10\ \mu\text{m}$, $j = 2.0\ \text{MA cm}^{-2}$ and $T = 473\ \text{K}$, and (3) Cho and Thompson (1989): $2w_0 = 2.2\ \mu\text{m}$, $L = 100\ \mu\text{m}$, $\ell_g = 6.5\ \mu\text{m}$, $j = 1.2\ \text{MA cm}^{-2}$ and $T = 548\ \text{K}$ in bamboo structures. In the computer simulations plotted in this figure the void surface diffusion coefficient $D_\sigma = 3.0 \times 10^{-6}\exp(-0.62\ \text{eV}/kT)\ \text{m}^2\ \text{s}^{-1}$ and the effective value of $\tilde{Z} = 4$ is chosen by reevaluating the experimental MTTF versus temperature data presented by three different authors (Lytle and Oates, 1992; Black, 1969; Schreiber and Grabe, 1981). Moreover it is assumed that the interfacial layer is one monolayer thick ($h = 2.86 \times 10^{-10}\ \text{m}$). The expression for the surface diffusivity is very close to the value reported for bulk

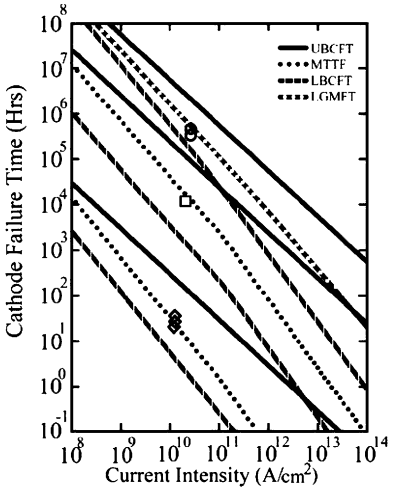

Fig. 9. Cathode failure time vs. current intensity graph on a double-logarithmic scale. ○: Longworth and Thompson (1992); □: Kinsbron (1980); ◇: Cho and Thompson (1989).

mono-vacancy diffusion in aluminum, namely: $D_b^{1V}(Al) = 1.66 \times 10^{-6} \exp(-0.62\ \mathrm{eV}/kT)\ \mathrm{m^2\ s^{-1}}$. This value can be deduced from the bulk diffusion constant $D_b(Al) = 3.7 \times 10^{-6}\ \mathrm{m^2\ s^{-1}}$ and the entropy of mono-vacancy formation $E^{1V,F} = 0.8k$ as reported by Seeger and Mehrer (1969). However, it will be shown that this agreement is coincidental and there is no connection between the vacancy bulk diffusion coefficient which involves only the activation enthalpy of motion, and the thermally activated surface diffusivity that has an activation energy which is the sum of the motional $E_\sigma^{1V,M}$ and formational $E_\sigma^{1V,F}$ activation enthalpies of thermal vacancies situated just at the surface layers.

The results in Fig. 9 show excellent agreement between theory and experiment with the exception being the case of a bi-crystal. The experimental results are selected from two different laboratories that utilize completely different microstructures, current densities and temperatures. For bamboo and near-bamboo structures the correlation between theoretical and experimental MTTF values are almost perfect. In the case of bi-crystals, experimental points lie at the midpoints of the UBCFT and LBCFT curves on the logarithmic scale. The bi-crystal MTTF formula given by Eq. (72) is exactly equivalent to the expression for the LBCFT. Therefore the logarithmic mean value of the LBCFT and UBCFT expressions may be used and is denoted as LGMFT in Fig. 9. This line yields a better prediction then the MTTF expression. Unfortunately, the published experimental observations have been performed on test specimens in which the microstructure has not been sufficiently characterized. The relationships for the LBCFT and the MTTF that include the current crowding region clearly show that the apparent current exponent varies from $n = -1$ to $n = -1.5$ for low and high current density domains, respectively. A smooth transition point is exhibited at 0.1 MA $\mathrm{cm^{-2}}$. For a given material the transition point only depends on the interconnect line width which can easily be predicted from Eq. (70). An interconnect having a larger line width prefers to have a lower current density transition point than one with a small interconnect line width.

As can be observed from Fig. 9 the MTTF reported by Longworth and Thompson (1992) for $\Sigma 13[100]$ and (115)/(100) bi-crystals are in agreement with our LGMFT prediction. However, it seems that this agreement is fortuitous because the appearance and location of failure sites observed by Longworth and Thompson (1992) indicate that the failure mechanism is likely to involve accelerated grain boundary grooving induced by electromigration. The experimental observations by Kinsbron (1980) on large blocking grains and by Cho and Thompson (1989) on bamboo structures are also studied and presented in Fig. 9. The results illustrate the prediction power of the MTTF concept. The current exponents for the LBCFT lines as illustrated in Fig. 9 are found to be approximately $n = -1.53$, which depends upon the choice of internal and external system variables.

Similarly, the UBCFT for the selected interconnect system parameters presented in Fig. 9, clearly indicates that the difference between the LBCFT and UBCFT increases with the current density. The current exponents for the UBCFT lines are found to be exactly $n = -1$ and the UBCFT lines are in agreement with the experimentally observed upper bond for the lognormal distribution of failure times for a wide variety of microstructures. According to the expressions for $s(\bar{w})$ reported above, the current exponent for the UBCFT should lie in the very narrow range $-1.058 \leqslant n \leqslant -1$, depending upon the current intensity and especially the grain size.

When the values of the diffusion coefficients in connection with the experimental data analysis in Figs. 8 and 9 are compared, it is found that they are in agreement up to a factor of three. It appears that the activation enthalpies obtained for both cases in Figs. 8 and 9 are very close to the activation enthalpy of motion of the bulk mono-vacancies in aluminum as reported by Seeger and Mehrer (1969). However, this argument is again fortuitous as can easily be verified by close inspection of the D_0 values associated with bulk mono-vacancies $D_b^{0,1V} = 1.66 \times 10^{-6}\ \mathrm{m^2\ s^{-1}}$, and with void surface drift-diffusivity $D_\sigma^0 = (1.10 \approx 3.0) \times 10^{-6}\ \mathrm{m^2\ s^{-1}}$. If there is an analytical connection between these two quantities, because of the existence of a high concentration of athermal vacancies generated during the recovery stage of the residual thermal stresses, this should be reflected in the diffusion constant $D_\sigma^0 = N_\sigma^{V,A} \times D^{0,1V}$, where $N_\sigma^{V,A}$ is the athermal or the excess vacancy concentration given in terms of atomic fraction at the void interfacial layer. This

relationship requires that the atomic fraction of excess vacancies at the void surface layer should be unusually large, i.e. at least 10% when considering the uncertainties in the adapted value $\hat{Z} = 4$ and in the thickness of the interfacial layer, which is assumed to be one monolayer, $h = 2.86 \times 10^{-10}$ m. The upper bound on the deformation induced or residual thermal stress induced excess vacancy concentration in metals is on the order of $N^{V}_{\mathrm{Def}} \approx 3 \times 10^{-4}$. This value can be produced by severe plastic deformation, as reported by Ogurtani (1979) from X-ray diffraction measurements in alpha brass, and also theoretically as predicted by Seeger (1957) utilizing a growing barrier model.

One can also use the argument of Schreiber (1981) based on a chemical bond picture and coordination number concept, that gives a mono-vacancy activation enthalpy of motion for an ideal oxygen free surface such as the (1 1 1)-plane as $H^{1\mathrm{V,M}}_{\sigma} = 5/12 E_{\mathrm{bond}} = 0.28$ eV, where the bond energy of aluminum is $E_{\mathrm{bond}} \cong 0.672$ eV. Schreiber claimed that thermal vacancies are not important if in the presence of athermal vacancies on surfaces, and he neglected them in his model calculations. However, to the contrary, thermal vacancy formation enthalpy is $H^{1\mathrm{V,F}}_{\sigma} = 6/12 E_{\mathrm{bond}} = 0.316$ eV, because nine bonds are broken and three new bonds are formed in order to take an atom from the (1 1 1) surface and attach it on the top of the flat free surface. Hence, six net bonds are destroyed. The surface drift-diffusion activation energy (enthalpy), which is the sum of the activation enthalpies for motion and formation, is $H^{1\mathrm{V}}_{\sigma} = H^{1\mathrm{V,M}}_{\sigma} + H^{1\mathrm{V,F}}_{\sigma} = 0.616$ eV in this case. Similarly, diffusion constants may be calculated from the formula presented by Manning (1968) for arbitrary structures and this formula is easily adapted to surface or two-dimensional diffusion. Using this result the diffusion coefficient for a close packed (1 1 1) plane in an FCC structure is: $D^{0}_{\sigma} = 3/4(a_0^2 \gamma_{\mathrm{D}}) \exp(S^{1\mathrm{V,M}}_{\sigma} + S^{1\mathrm{V,F}}_{\sigma}/k)$, where $a_0 \cong 4.04 \times 10^{-10}$ m is the lattice parameter, $\gamma_{\mathrm{D}} \cong 8.12 \times 10^{12}\, s^{-1}$ is the Debye frequency (Seitz, 1940), $S^{1\mathrm{V,M}}_{\sigma} \cong 0.2k$ is the entropy of motion of mono-vacancies obtained by the present authors using the value of D_{10} reported by Seeger and Mehrer (1969) and $S^{1\mathrm{V,F}}_{\sigma} \cong 0.8k$ is the entropy of formation of mono-vacancies, valid in aluminum (Seeger and Mehrer, 1969). The data for bulk aluminum results in a diffusion constant $D^{0}_{\sigma} \cong 2.74 \times 10^{-6}$ m^2 s^{-1}, which is in excellent agreement with the value obtained in the analysis of the experimental data for interconnects with bamboo structures shown in Fig. 8. If it is assumed that the bulk Debby frequency and the motional and formational entropies for bulk diffusion are extrapolated as first order approximations for the surface states, as assumed in the above calculations, inspection of the formula presented above yields the identity $D^{0}_{\sigma}(111) = 3/4 \cdot D^{0,1\mathrm{V}}_{\mathrm{b}}$ (FCC).

According to the relationship for the UBCFT, which is the only expression presented above that explicitly includes the linear line width $2w_0$, the dependence of which is not in accord with the suggestion made by Arzt et al. (1996) for bamboo structures. Similarly the MTTF formulas, which implicitly include the line width dependence in the current crowding region through the critical radius and the current exponents, is not in agreement with the suggestion of Arzt et al. (1996). However, the formulae show some common behavior, namely that any increase in line width results in a similar increase in the cathode failure time. Arzt and his coworkers found that as w_0 is decreased, the MTTF decreases to a minimum and then increases continuously having a turning point at $2w_0/\ell_{\mathrm{g}} \cong 2$. Arzt et al. (1996) clearly state that when the grain size and the line width are comparable, a 'near bamboo' structure results with strong flux divergences at the ends of the polycrystalline segments. Therefore, it is speculated that in the studies of Cho and Thompson (1989) where the grain size is less than the line width the region should be considered polycrystalline rather than a simple bamboo structure as suggested by Arzt and his coworkers (1996). Eq. (73) also reveals that the mean lifetime is directly proportional to the interconnect line length or the stud to stud distance.

A value of $n = -2$ as a current exponent was predicted by Black (1969) based on the assumption that the momentum transfer from electrons to Al atoms is proportional to the Al flux and to the drift velocity of electrons. However, this assumption contradicts the commonly accepted atomistic description of electron transport (Wever, 1973). More rigorous derivations of the value $n = -2$ by Shatzkes and Lloyd (1986), Basaran et al. (2003) and Kirchheim and Kaeber (1991) rely on the assumption that the time necessary to attain a super saturation of vacancies in a semi-infinite Al line is equal to the median time to failure, MTTF. Kirchheim and Kaeber (1991) also observed that if the MTTF values are plotted as a function of the current

density j instead of the reduced current density $(j-j_{crit})$ in a log–log plot the slope $n=-3/2$. All of these model calculations assume that the interconnect failure takes place at the cathode pad (or stud) by the accumulation or creation of voids in that region. Therefore, the failure mechanisms associated with slit or wedge shape defect formation by the growth of inter or edge voids as they migrate along the interconnect are completely ignored by these authors (Black, 1969; Shatzkes and Lloyd, 1986; Kirchheim and Kaeber, 1991).

Experimentally measured current density exponents reported for polycrystalline aluminum in the literature (Arzt et al., 1996; Joo and Thompson, 1997) show a rather wide range of values $|n|=1$–6 depending upon the alloying elements, the microstructure, the processing and service conditions, and the method of data analysis. In our previous paper (Ogurtani and Oren, 2001) it has been demonstrated that if transgranular failure of a single crystal is controlled by void motion or growth but not the nucleation of voids then the current exponent $n=-1$. According to Joo and Thompson (1997) and Arzt et al. (1996) the current-density dependence of the MTTF of a single-crystal Al conductor line reveals that the exponent n is closer to -2 rather than -1 and the activation enthalpy of the process is about 1.0 eV. The measured value of the current exponent caused them to speculate in their experimental studies that nucleation of the void is the rate controlling step rather than void motion and growth. In order to explain an activation enthalpy of this magnitude, which does not coincide with any known drift-diffusion paths, these authors made the additional conjecture that the drift-diffusion path goes through the interfacial layer between Al and Al_2O_3. However, Schreiber (1981) clearly states that no one has measured the electromigration kinetics at the technical surfaces such as the (Al–Al_2O_3) interface. The careful measurements by Schafft et al. (1985) on Al lines covered with SiO_2 passivation layers reveal the effect of heating on n. By knowing the temperature increase of the line they were able to subtract its contribution from the measured MTTF, and obtained the value $n\cong -3/2$. Liu et al. (2001) obtained exactly the same current exponent n for the void growth rate, as it propagates along the grain boundary in interconnects with applied electrical current. Similarly Suo et al. (1994) and Klinger et al. (1996) found that the slit propagation speed is proportional to $E_0^{3/2}$, which yields an equivalent current exponent since the MTTF is inversely proportional to the propagation velocity.

The dependence of the current density on Eq. (73), which is directly applicable to the case in which there are preexisting (stress induced) over-critical size voids, indicates that there may be two different regimes. The two regimes result in completely different current exponents at moderate and/or high current densities but yield exactly the same exponent $n\cong -1$ in the current crowding domain. Current crowding always prevails at low current density ($j\leqslant 0.1$ MA cm^{-2}). The first regime is governed by the first term, namely the detachment term, and the second regime is controlled by the second term, that is, the mean flight time of a void before it reaches the cathode pad or stud.

5. Conclusions

The present computer simulation study has produced fundamental and analytical laws relating void–grain boundary detachment time and the threshold level of the normalized electron wind intensity at the onset of the detrapping process. These laws are combined to produce three important and technologically useful relationships for the evaluation of the MTTF and the upper and lower bonds for the life time of an interconnect, in terms of the applied current density, the surface diffusivity, and structural parameters such as grain size, line width and the interconnect stud to stud length.

Another important outcome of this study is the inspection of a general tendency of strongly distorted voids to breakup. Void breakup has been observed experimentally (Madden et al., 1992), and it should be beneficial to the stability of the line because it counteracts the growth of voids by coalescence. From a theoretical perspective, topological transitions such as void fragmentation and breakup or the merging of a void with a boundary are the most intriguing aspects of this novel, largely unexplored moving boundary value problem (Joo and Thompson, 1997).

This model, however still does not take into account explicitly the incubation time for the homogeneous nucleation of interior voids, since it is assumed that the rate controlling unit processes are void detachment from the grain boundaries and void migration kinetics between two successive boundaries. Therefore, if the heterogeneous nucleation of the edge voids at the intersection (triple junction) between bamboo grain boundary and the technical surface of the interconnect could be suppressed then substantial improvement in the failure life time may be realized. One way of achieving this objective would be to sputter a hot coating layer on the cold interconnect substrate that would generate residual compressive stresses at the technical surfaces at the device operating temperature. This would inhibit vacancy clustering and eventual void nucleation at the specimen edges and triple junctions. An order of magnitude enhancement has been obtained by Arzt et al. (1996) in Al–Si–Cu interconnects by utilizing hot-sputtering conditions, rather than cold-sputtering. This justifies our speculation that compressive stresses at the technical surface are an important agent for inhibition of heterogeneous nucleation, which improves the service life of the interconnects.

The present theory may be very useful in developing full knowledge of the surface diffusivities by furnishing not only the activation enthalpies but also the diffusion constants. Analysis of numerous experimental data cited in this paper (Black, 1969; Longworth and Thompson, 1992; Kinsbron, 1980; Cho and Thompson, 1989; Seeger and Mehrer, 1969; Ogurtani, 1979) gives very consistent and highly accurate values for the surface diffusion constant $D_\sigma^0 = 3.0 \times 10^{-6}\ \mathrm{m^2\ s^{-1}}$ and the enthalpy $H_\sigma^{1V} = 0.62\ \mathrm{eV}$ if one assumes that $\tilde{Z}(Al) = 4$ for voids formed in the interior of the aluminum interconnects avoiding any interface contamination such as oxides. These values are unusually close to those values calculated in this paper by utilizing a simple model based on coordination numbers supplemented by a bond-breaking and forming model as applied to mono-vacancies created at (1 1 1) planes of clean or freshly formed aluminum surfaces. Therefore, by analyzing the behavior of the LBCFT and the MTTF as a function of temperature and current density data, the simulations reveal that the inner void failure mechanism is solely controlled by thermal mono-vacancy diffusion along the void interface. This result means that even though there might be substantial bulk mono-vacancy saturation in test specimens reported in the literature void surface diffusion kinetics is still controlled solely by the concentration of thermal surface vacancies.

Similarly, in those interconnect specimens where failure occurs by voids initially nucleated at the intersections of the technical surfaces with the grain boundaries, (triple junctions) and which subsequently penetrate into the interior of the specimen through the grain boundaries (Marieb et al., 1995), the evolution kinetics exhibit completely different drift-diffusion parameters. Because of the contamination of the technical surface by impurities such as oxygen, the vacancy activation enthalpy of motion involves the additional contribution of the enthalpy of binding of vacancies to trap centers. In the case of aluminum, our analysis of the experimental data reported by Black (1969) for large crystallites and Lytle and Oates (1992) for specimens without voids indicates that there exists a completely different set of diffusion coefficients. These diffusion coefficients may be interpreted as drift-diffusion coefficients for athermal vacancies associated with the contaminated void surface mobilities. This discrepancy is due to the initial nucleation of the voids at the technical surfaces or at the specimen edges, which contain unavoidable trap centers for vacancies resulting in addition enthalpy (or binding energy) contributions to the diffusion activation energy of motion. The void and/or the surface drift-diffusion coefficients are found to be: $D_\sigma^{\mathrm{Void}} = 7.0 \times 10^{-6} \exp(-0.84\ \mathrm{eV}/kT)\ \mathrm{m^2\ s^{-1}}$ and $D_\sigma^{\mathrm{Surface}} = 6.0 \times 10^{-6} \exp(-0.84\ \mathrm{eV}/kT)\ \mathrm{m^2\ s^{-1}}$, respectively. The binding energy of mono-vacancies to oxygen trap centers at the technical surfaces is estimated to be $H_\sigma^{1V,B} = 0.22\ \mathrm{eV}$.

Acknowledgments

The senior author has the great pleasure to dedicate this paper to his professors, the late Professors Eric Hutchinson and van Rysselberghe of Stanford University who inspired him to learn deep insight of many facets of thermodynamics. The authors also wish to thank Professors William D. Nix of Stanford University,

and Macit Özenbaş of METU for their very valuable suggestions and encouraging interest in the initiation of this extensive research program at METU. Finally, Professor Lucien N. Brush of University of Washington has our heartfelt gratitude for ensuring the text clearly conveys our message to the readers.

References

Arzt, E., Kraft, O., Spolenak, R., Joo, Y.C., 1996. Physical metallurgy of electromigration: Failure mechanisms in miniaturized conductor. Z. Metallkd. 87 (11), 934–942.

Averbuch, A., Israeli, M., Nathan, M., Ravve, I., 2003a. Surface evolution in bare bamboo-type metal lines under diffusion and electric field effects. J. Comput. Phys. 188 (2), 640–677.

Averbuch, A., Israeli, M., Ravve, I., 2003b. Electromigration of intergranular voids in metal films for microelectronic interconnects. J. Comput. Phys. 186 (2), 481–502.

Bakker, G., 1911. Theorie de la couche capillaire plane dans les corps purs. Gauthier-Villars, Paris, p.74.

Basaran, C., Lin, M., Ye, H., 2003. A thermodynamic model for electrical current induced damage. Int. J. Solids Struct. 40, 7315–7327.

Black, J.R., 1969. Electromigration failure modes in aluminum metallization for semiconductor devices. Proc. IEEE 57 (9), 1587.

Buff, F.P., 1955. Spherical interface. II. Molecular theory. J. Chem. Phys. 23 (3), 419–426.

Cahn, J.W., Hilliard, J.E., 1958. Free energy of a nonuniform system. I. Interfacial free energy. J. Chem. Phys. 28 (2), 258–267.

Cahn, J.W., Elliott, C.M., Novick-Cohen, A., 1996. The Cahn–Hilliard equation with a concentration dependent mobility: motion by minus the Laplacian of the mean curvature. Eur. J. Appl. Math. 7, 287–301.

Callen, H.B., 1960. Thermodynamics. John Wiley & Sons, New York, p. 237.

Cho, J., Thompson, C.V., 1989. Grain size dependence of electromigration-induced failures in narrow interconnects. Appl. Phys. Lett. 54 (25), 2577–2579.

Chuang, T.J., Rice, J.R., 1973. Shape of intergranular creep cracks growing by surface diffusion. Acta Metall. Mater. 21 (12), 1625–1628.

Chuang, T.J., 1983. On the energy–release rate associated with diffusional crack-growth. Int. J. Fract. 23 (3), 229–242.

Cocks, A.C.F., 1994. The structure of constitutive laws for the sintering of fine-grained materials. Acta Metall. Mater. 42 (7), 2191–2210.

De Groot, S.R., 1951. Thermodynamics of Irreversible Processes. North-Holland, Amsterdam, p. 27.

Defay, R., Prigogine, I., Bellemans, A., 1966. Surface Tension and Adsorption. John Wiley & Sons, New York, p. 363.

Donder, T.D., van Rysselberghe, P., 1936. Affinity. Stanford University Press, Menlo Park, p. 12.

Fung, Y.C., 1965. Foundation of Solid Mechanics. Prentice-Hall, New Jersey, p. 349.

Gibbs, W., 1948. The collected works of J. Willard GibbsThermodynamics, vol. I. Yale University Press, New Haven, p. 226.

Gottstein, G., Shvindlerman, L.S., 2002. Triple junction drag and grain growth in 2D polycrystals. Acta Mater. 50 (4), 703–713.

Guggenheim, E.A., 1959. Thermodynamics, fourth ed. North-Holland, Amsterdam, p. 39.

Gungor, M.R., Maroudas, D., 2001. Modeling of electromechanically-induced failure of passivated metallic thin films used in device interconnections. Int. J. Fract. 109 (1), 47–68.

Haase, R., 1969. Thermodynamics of Irreversible Processes. Addison-Wesley, Massachusetts, p. 245.

Herring, C., 1951. In: Kinston, W.E. (Ed.), The Physics of Powder Metallurgy. McGraw-Hill, New York, p. 143.

Ho, P.S., 1970. Motion of inclusion induced by a direct current and a temperature gradient. J. Appl. Phys. 41 (1), 64.

Huang, P.Z., Li, Z.H., Sun, J., 2000. Finite-element simulation of the diffusive growth of grain boundary voids. Model. Simul. Mater. Sci. Eng. 8 (6), 843–856.

Joo, Y.C., Thompson, C.V., 1997. Electromigration-induced transgranular failure mechanisms in single-crystal aluminum interconnect. J. Appl. Phys. 81 (9), 6062–6072.

Kazaryan, A., Wang, Y., Patton, B.R., 1999. Generalized phase field approach for computer simulation of sintering: incorporation of rigid-body motion. Scr. Mater. 41 (5), 487–492.

Khenner, M., Averbuch, A., Israeli, M., Nathan, M., 2001. Numerical simulation of grain-boundary grooving by level set method. J. Comput. Phys. 170 (2), 764–784.

Kinsbron, E., 1980. A model for the width dependence of electromigration lifetimes in Al thin-film stripes. Appl. Phys. Lett. 36 (12), 968–970.

Kirchheim, R., Kaeber, U., 1991. Atomistic and computer modeling of metallization failure of integrated-circuits by electromigration. J. Appl. Phys. 70 (1), 172–181.

Klinger, L.M., Chu, X., Mullins, W.W., Bauer, C.L., 1996. Grain-boundary slit propagation in an electric field. J. Appl. Phys. 80 (12), 6670–6676.

Kucherenko, S., Pan, J., Yeomans, J.A., 2000. A combined finite element and finite difference scheme for computer simulation of microstructure evolution and its application to pore-boundary separation during sintering. Comput. Mater. Sci. 18 (1), 76–92.

Landau, L.D., Lifshitz, E.M., 1980. Statistical Physics. Pergamon Press, Oxford, Part II, p. 178.
Laplace, P.S., 1806. Mechanique ceileste. suppl. au X Livre, Impr. Imeriale, vol. 10, p. 147.
Liang, J., Suo, Z., 2001. Stress-assisted reactions at a solid–fluid interface. Interface Sci. 9 (1–2), 93–104.
Liu, C.Y., Lee, S., Chuang, T.J., 2001. Grain boundary crack growth in interconnects with an electric current. Mater. Sci. Eng. B—Solid 86 (2), 101–108.
Longworth, H.P., Thompson, C.V., 1992. Experimental study of electromigration in bicrystal Al lines. Appl. Phys. Lett. 60 (18), 2219–2221.
Lytle, S.A., Oates, A.S., 1992. The effect of stress-induced voiding on electromigration. J. Appl. Phys. 71 (1), 174–178.
Madden, M.C., Abratowski, E.V., Marieb, T., Flinn, P.A., 1992. High resolution observation of void motion in passivated metal lines under electromigration stress. Mater. Res. Soc. Symp. Proc. 265, 33–38.
Mahadevan, M., Bradley, R.M., 1999. Phase field model of surface electromigration in single crystal metal thin films. Physica D 126 (3–4), 201–213.
Manning, J.P., 1968. Diffusion Kinetics for Atoms in Crystals. D. van Nostrand, Princeton, p. 43.
Marieb, T., Flinn, P., Bravman, J.C., Gardner, D., Madden, M., 1995. Observations of electromigration-induced void nucleation and growth in polycrystalline and near-bamboo passivated Al lines. J. Appl. Phys. 78 (2), 1026–1032.
Mullins, W.W., 1957. Theory of thermal grooving. J. Appl. Phys. 28 (3), 333–339.
Mullins, W.W., 2001. Capillarity-induced surface morphologies. Interface Sci. 9 (1–2), 9–20.
Murr, L.E., 1975. Interfacial Phenomena in Metals and Alloys. Addison-Wesley, Massachusetts, p. 10.
Needleman, A., Rice, J.R., 1980. Plastic creep flow effects in the diffusive cavitation of grain-boundaries. Acta Metall. Mater. 28, 1315–1332.
Novick-Cohen, A., 2000. Triple-junction motion for an Allen-Cahn/Cahn–Hilliard system. Physica D 137 (1–2), 1–24.
Ogurtani, T.O., 1979. Kinetics of atomic diffusion to stacking-faults and the related special problems in cold-worked alpha-brasses. Metall. Trans. A. 10 (10), 1505–1513.
Ogurtani, T.O., 1989. Cherenkov-type sharp energy-dissipation associated with kinks (solitons) moving harmonically in the atmosphere of paraelastic interstitial atmosphere. J. Appl. Phys. 66 (11), 5274–5277.
Ogurtani, T.O., 2000. Irreversible thermokinetics theory of surfaces and interfaces with a special reference to triple junctions (unpublished).
Ogurtani, T.O., Akyildiz, O., 2004. Grain boundary grooving and cathode voiding in bamboo-like metallic interconnects by surface drift-diffusion under the capillary and electromigration forces (unpublished).
Ogurtani, T.O., Oren, E.E., 2001. Computer simulation of void growth dynamics under the action of electromigration and capillary forces in narrow thin interconnects. J. Appl. Phys. 90 (3), 1564–1572.
Ogurtani, T.O., Seeger, A.K., 1985. Dislocation-enhanced induced Snoek peak associated with heavy interstitials in the presence of kinks moving harmonically in anistropic body-centered-cubic metals. Phys. Rev. B 31 (8), 5044–5057.
Ogurtani, T.O., Seeger, A.K., 1987. Nonlinear-theory of the dislocations-enhanced Snoek effect and its connection with the geometric and/or thermal kink oscillations on nonscrew dislocations in body-centered-cubic metals. J. Appl. Phys. 62 (9), 3704–3711.
Ohring, M., 1971. Electromigration damage in thin films due to grain boundary grooving processes. J. Appl. Phys. 42 (7), 2653–2661.
Ono, S., Kondo, S., 1960. Encyclopedia of Physics, vol. X. Flügge, Berlin, p. 159.
Oren, E.E., Ogurtani, T.O., 2002. Void intergranular motion under the action of electromigration forces in thin film interconnects with bamboo structure. Mater. Res. Soc. Symp. Proc. 695, L.5.5.1.
Pan, J., Cocks, A.C.F., 1994. A constitutive model for stage-2 sintering of fine-grained materials. 1. Grain-boundaries act as perfect sources and sinks for vacancies. Acta Metall. Mater. 42 (4), 1215–1222.
Pan, J., Cocks, A.C.F., 1995. A numerical technique for the analysis of coupled surface and grain-boundary diffusion. Acta Metall. Mater. 43 (4), 1395–1406.
Pharr, G.M., Nix, W.D., 1979. Numerical study of cavity growth controlled by surface diffusion. Acta Metall. Mater. 27, 1615–1631.
Prigogine, I., 1961. Introduction to Thermodynamics of Irreversible Processes. Interscience, New York, p. 29.
Rice, J.R., Chuang, T.J., 1981. Energy variations in diffusive cavity growth. J. Am. Ceram. Soc. 64 (1), 46–53.
Schafft, H.A., Grant, T.C., Saxena, A.N., Kao, C.Y., 1985. Electromigration and the current density dependence. IEEE Proc. Int. Rel. Phys. 23, 93.
Schimschak, M., Krug, J., 2000. Electromigration-driven shape evolution of two-dimensional voids. J. Appl. Phys. 87 (2), 695–703.
Schreiber, H.U., 1981. Activation-energies for the different electromigration mechanisms in aluminum. Solid-State Electron. 24, 583.
Schreiber, H.U., Grabe, B., 1981. Electromigration measuring techniques for grain-boundary diffusion activation-energy in aluminum. Solid-State Electron. 24, 1135–1146.
Seeger, A.K., 1957. Dislocations and the Mechanical Properties of Crystals. John Wiley & Sons, New York, p. 243.
Seeger, A.K., Mehrer, H., 1969. In: Seeger, A.K., Schumacher, D., Shilling, W., Diehl (Eds.), Vacancies and Interstitials in Metals. North-Holland, Amsterdam, pp. 1–58.
Seitz, F., 1940. The Modern Theory of Solids. McGraw-Hill, New York, p. 110.

Shatzkes, M., Lloyd, J.R., 1986. A model for conductor failure considering diffusion concurrently with electromigration resulting in a current exponent of 2. J. Appl. Phys. 59 (11), 3890–3893.

Suo, Z., Wang, W., 1994. Diffusive void bifurcation in stressed solid. J. Appl. Phys. 76 (6), 3410–3421.

Suo, Z., Wang, W., Yang, M., 1994. Electromigration instability-transgranular slits in interconnects. Appl. Phys. Lett. 64 (15), 1944–1946.

Takahashi, Y., Takahashi, K., Nishiguchi, K., 1991. A numerical-analysis of void shrinkage processes controlled by coupled surface and interface diffusion. Acta Metall. Mater. 39 (12), 3199–3216.

van der Waals, Baker, J.D., 1928. Handbook Experimental Physik, vol. 6. Springer-Verlag, Berlin, p. 22.

Verschaffelt, J.E., 1936. The thermomechanics of the superficial layer. I. Generalities; pure substances. Bull. Sci. Acad. Roy. Belg. 22, 373.

Von-Neumann, J., 1952. Metal Interfaces. ASM, Cleveland, p. 108.

Wang, W.Q., Suo, Z., 1996. A simulation of electromigration-induced transgranular slits. J. Appl. Phys. 79 (5), 2394–2403.

Wever, H., 1973. Elektro-und Thermotransporten in Metallen. Johann Ambrosius Barth, Leibzig, p. 89.

Yeremin, E.N., 1979. The Foundation of Chemical Kinetics. MIR Publishers, Moscow, p. 215.

Young, T., 1805. An essay on the cohesion of fluids. Philos. Trans. R. Soc. London 95, 65.

Zhang, Y.W., Bower, A.F., 2001. Three-dimensional analysis of shape transitions in strained-heteroepitaxial islands. Appl. Phys. Lett. 78 (18), 2706–2708.